

Hybrid Transceiver Design for Tera-Hertz MIMO Systems Relying on Bayesian Learning Aided Sparse Channel Estimation

Suraj Srivastava, *Student Member, IEEE*, Ajeet Tripathi, Neeraj Varshney, *Member, IEEE*,

Aditya K. Jagannatham, *Member, IEEE*, and Lajos Hanzo, *Fellow, IEEE*

Abstract

Hybrid transceiver design in multiple-input multiple-output (MIMO) Tera-Hertz (THz) systems relying on sparse channel state information (CSI) estimation techniques is conceived. To begin with, a practical MIMO channel model is developed for the THz band that incorporates its molecular absorption and reflection losses, as well as its non-line-of-sight (NLoS) rays associated with its diffused components. Subsequently, a novel CSI estimation model is derived by exploiting the angular-sparsity of the THz MIMO channel. Then an orthogonal matching pursuit (OMP)-based framework is conceived, followed by designing a sophisticated Bayesian learning (BL)-based approach for efficient estimation of the sparse THz MIMO channel. The Bayesian Cramer-Rao Lower Bound (BCRLB) is also determined for benchmarking the performance of the CSI estimation techniques developed. Finally, an optimal hybrid transmit precoder and receiver combiner pair is designed, which directly relies on the beamspace domain CSI estimates and only requires limited feedback. Finally, simulation results are provided for quantifying the improved mean square error (MSE), spectral-efficiency (SE) and bit-error rate (BER) performance for transmission on practical THz MIMO channel obtained from the HIGH resolution TRANsmission (HITRAN)-database.

Index Terms

Bayesian learning, beamspace representation, HITRAN-database, hybrid MIMO systems, molecular absorption, sparse channel estimation, tera-Hertz communication, transceiver design

I. INTRODUCTION

Tera-Hertz (THz) wireless systems are capable of supporting data rates up to several Tera-bits per second (Tbps) [1]–[3] in the emerging 6G landscape. The availability of large blocks

S. Srivastava, A. Tripathi and A. K. Jagannatham are with the Department of Electrical Engineering, Indian Institute of Technology Kanpur, India-208016 (e-mail: {ssrivast, tajeet, adityaj}@iitk.ac.in). N. Varshney is with the Wireless Networks Division, National Institute of Standards and Technology (NIST), Gaithersburg, MD 20899-6730, USA (E-mail: neerajv@ieee.org). L. Hanzo is with the School of Electronics and Computer Science, University of Southampton, Southampton SO17 1BJ, U.K. (e-mail: lh@ecs.soton.ac.uk).

of spectrum in the THz band, in the range of 0.1 THz to 10 THz, can readily fulfil the ever-increasing demand for data rates. This can in turn support several bandwidth-thirsty applications such as augmented reality (AR), virtual reality (VR), wireless backhaul and ultra-high speed indoor communication [1]. However, due to their high carrier frequency, THz signals experience severe propagation losses and blockage, beyond a few meters. Moreover, the high molecular absorption due to the vibrations of the molecules at specific frequencies, and the higher-order reflections [4] become cumbersome in the THz band. Hence, the practical realization of THz systems faces numerous challenges. A promising technique of overcoming these obstacles is constituted by multiple-input multiple-output (MIMO) solutions relying on antenna arrays, which are capable of improving the signal strength at the receiver via the formation of ‘pencil-sharp beams’ having ultra-high directional gains [5]. However, the conventional MIMO transceiver architecture, wherein each transmit and receive antenna is connected to an individual radio frequency (RF) chain, becomes unsuitable at such high frequencies, mainly due to the power hungry nature of the analog-to-digital converters coupled with their high sampling-rate [6]. Hence, the hybrid transceiver architecture, originally proposed by Molish *et al.* in their pioneering work [7], [8], is an attractive choice for such systems, since it allows the realization of a practical transceiver employing only a few RF chains. Furthermore, in conventional MIMO systems, the various signal processing operations are typically implemented in the digital domain. By contrast, the signal processing tasks are judiciously partitioned between the RF front-end and baseband processor in a hybrid MIMO transceiver, with the former handling the analog processing via analog phase shifters (APSs), while the latter achieves baseband processing in a digital signal processor (DSP). Naturally, the overall performance of the hybrid architecture, for example, its achievable spectral-efficiency (ASE) and bit-error-rate (BER), critically depend on the design of the baseband and RF precoder/ combiner, which ultimately relies on the accuracy of the available channel state information (CSI). Thus, high-precision channel estimation holds the key for attaining robust performance and ultimately for realizing the full potential of THz MIMO systems. A detailed overview and a comparative survey of the related works is presented next.

A. Related Works and Contributions

The pioneering contribution of Jornet and Akyildiz [4] developed a novel channel model for the entire THz band, i.e. for the band spanning 0.1 – 10 THz. Their ground-breaking work relied on the concepts of radiative transfer theory [9] and molecular absorption for developing a

comprehensive model [10]. Their treatise evaluated the total path-loss by meticulously accounting for the molecular absorption, the reflections as well as for the free-space loss components. Later Yin and Li [11] developed a general MIMO channel model for a hybrid THz system and subsequently proposed distance-aware adaptive beamforming techniques for improving the signal-to-noise power ratio (SNR). However, their framework assumes the availability of perfect CSI, which is rarely possible in practice. To elaborate, CSI estimation in a THz hybrid MIMO system is extremely challenging owing to the low SNR and massive number of antenna elements. Hence, the conventional Least Square (LS) and Minimum Mean Square Error (MMSE)-based CSI estimation would incur an excessive pilot-overhead. Therefore, they are unsuitable for CSI acquisition in practical THz systems.

Early solutions [12]–[19] proposed for the milli-meter wave (mmWave) band exploited the angular-sparsity of the channel to achieve improved CSI estimation and tracking at a substantially reduced pilot-overhead. Several optimization and machine learning based algorithms are also proposed for hybrid transceiver design in mmWave MIMO systems. In this context, the authors of [20] proposed joint beam selection and precoder design for maximizing the sum-rate of a downlink multiuser mmWave MIMO system under transmit power constraints. The pertinent optimization problem has been formulated as a weighted minimum mean squared error (WMMSE) problem, which is then efficiently solved using the penalty dual decomposition method. A joint hybrid precoder design procedure has been described in [21] for full-duplex relay-aided multiuser mmWave MIMO systems, considering also the effects of imperfect CSI. The authors of [22] and [23] successfully developed two-timescale hybrid precoding schemes for maximizing the sum-rate, and reducing the complexity and CSI feedback overhead. A frame-based transmission scenario is considered in their work, wherein each frame comprises a fixed number of time slots. The long-timescale RF precoders are designed based on the available channel statistics and are updated once in a frame. By contrast, the short-timescale baseband precoders are optimized for each time slot based on the low-dimensional effective CSI. Hence, an optimization based solution is developed in [22], whereas a deep neural network (DNN)-aided technique is designed in [23]. The angular-sparsity is also a key feature of the THz MIMO channel [5], [24], which arises due to the highly directional beams of large antenna arrays, coupled with high propagation losses and signal blockage in the THz regime. In fact, Sarrideen *et al.* [5] showed that the THz MIMO channel is more sparse than its mmWave counterpart. However, there are only a few recent studies, such as [25]–[27], which develop sparse recovery based CSI estimation techniques for

THz MIMO systems. A brief review of these and the gaps in the existing THz literature are described next.

The early work of Gao *et al.* [28] successfully developed an *a priori* information aided fast CSI tracking algorithm for discrete lens antenna (DLA) array based THz MIMO systems. Their model relies on a practical user mobility trajectory [29] to develop a time-evolution based framework for the angle of arrival (AoA)/ angle of departure (AoD) of each user. Subsequent contributions in this direction, such as [30] and [31], consider base station (BS) cooperation and a multi-resolution codebook, respectively, for improving the accuracy of channel tracking obtained via the *a priori* information aided scheme of [28]. However, this improved tracking accuracy is achieved at the cost of inter-BS cooperation, which necessitates additional infrastructure and control overheads. Kaur *et al.* [32] developed a model-driven deep learning technique for enhancing the channel tracking accuracy in a THz MIMO system. Their algorithm relies on a deep convolutional neural network trained offline in advance to learn the non-linear relationship between the estimates based on [28] and the original channel. Another impressive contribution [6] by He *et al.* proposes a model-driven unsupervised learning network for beamspace channel estimation in wide-band THz MIMO systems. Furthermore, a deep learning assisted signal detection relying on single-bit quantization is proposed in the recent contribution [33]. A fundamental limitation of [28], [30]–[32] is that they consider single antenna users. More importantly, their estimation accuracy is highly sensitive to the accuracy of the time-evolution model employed and they do not incorporate the effect of molecular absorption into their THz channel, which renders the model inaccurate in reproducing the true radio propagation environment.

Schram *et al.* [26] employed an approximate message passing (AMP)-based framework for CSI estimation in THz systems. The sparse channel estimation framework developed considers only a single-input single-output (SISO) THz system, where the channel impulse response (CIR) is assumed to be sparse. Ma *et al.* [27] conceived sparse beamspace CSI estimation for intelligent reflecting surface (IRS)-based THz MIMO systems. The optimal design of the phase shift matrix at the IRS has been determined in their work based on the BS to IRS and IRS to user equipment (UE) THz MIMO channels. Recent treatises, such as [34]–[36], address the problem of wideband CSI acquisition in THz systems. Specifically, Dovelos *et al.* [34] consider an orthogonal frequency division multiplexing (OFDM)-based THz hybrid MIMO system and develop orthogonal matching pursuit (OMP)-based techniques for CSI estimation. Balevi and Andrews [36] have considered generative adversarial networks for channel estimation in an

TABLE I: Boldly contrasting our novel contributions to the state-of-the-art

Features	[4]	[6]	[11]	[27]	[32]	[28]	[26]	[36]	[34]	[35]	Proposed
THz hybrid MIMO			✓	✓				✓	✓		✓
APSSs-based hybrid architecture			✓	✓				✓	✓		✓
Single antenna users		✓	✓		✓	✓	✓		✓		✓
CSI estimation		✓		✓	✓	✓	✓	✓	✓	✓	✓
Diffused-ray modeling											✓
Angular-sparsity		✓	✓	✓		✓	✓		✓		✓
Molecular absorption losses	✓		✓						✓		✓
Reflection losses			✓						✓		✓
Optimal pilot design										✓	✓
Transceiver design				✓					✓		✓
Optimal power allocation			✓								✓
Limited CSI feedback											✓
MSE lower bound									✓	✓	✓

OFDM-based THz hybrid MIMO system. On the other hand, Sha and Wang [35] derived a CSI estimation and equalization technique for a single-carrier THz SISO system accounting also for realistic RF impairments. A list of novel contributions of our paper is presented next. Our novel contributions are also boldly and explicitly contrasted to the existing literature in Table-I.

B. Novel Contributions

- 1) We commence by developing a practical distance and frequency dependent THz MIMO channel model that also incorporates the molecular absorption and reflection losses together with the traditional free-space loss. Note that almost all the existing contributions utilize the classical Saleh-Valenzuela channel model of [37], which does not consider the diffused rays for each multipath component together with first- and second-order reflections. Furthermore, the path-gains in most of the existing treatises are simply modeled as Rayleigh fading channel coefficients without considering the molecular absorption and multiple reflections. Hence, an important aspect of the channel model developed is that it incorporates several diffused rays for each of the reflected multipath components including their associated reflection and molecular absorption losses. This results in broadening of the beamwidths of the signals and mimics a practical THz MIMO channel.

- 2) The existing research on the development of sparse CSI estimation schemes for a point-to-point analog phase shifter (APS) based hybrid MIMO THz system is very limited, since most of them have considered only single-antenna users, focusing predominantly on discrete lens antenna (DLA) arrays. Hence for considering a point-to-point APS-based hybrid MIMO architecture, an efficient frame-based channel estimation model is developed, which frugally employs a low number of pilot beams for exciting the various angular modes of the channel. Subsequently, using a suitable ‘sparsifying’-dictionary, a beamspace representation is developed for the THz MIMO channel, followed by the pertinent sparse channel estimation model. For this, BL-based channel estimation techniques are derived for exploiting the sparsity of the THz MIMO channel. Note that the proposed BL-based technique is novel in the context of THz MIMO channel estimation, since it has not been explored as yet in THz hybrid MIMO systems.
- 3) The design of the optimal pilot beams used for CSI estimation, which can significantly enhance sparse signal recovery, has not been considered in the existing THz literature either. Moreover, it is also desirable to develop bounds to benchmark the performance of the CSI estimation schemes. To this end, another key contribution of this work is the design of a specific pilot matrix that minimizes the so-called ‘total-coherence’¹ defined in [38], [39] for enhancing the performance of sparse signal recovery. Furthermore, to benchmark the MSE performance of our sparse CSI estimators, the Bayesian Cramer-Rao lower bound (BCRLB) is also derived for the CSI estimates.
- 4) To the best of our knowledge, the existing hybrid transceiver design approaches found in the THz literature, such as [40], assume the availability of perfect CSI, which is impractical due to the large number of antennas, resulting in excessive pilot overheads. Crucially, no joint beamspace channel estimation and hybrid transceiver design procedure is available in the THz literature. To address this problem, a capacity-approaching hybrid transmit precoder (TPC) and MMSE-optimal hybrid receiver combiner (RC) are developed, which can directly employ the estimate of the beamspace domain channel obtained from the proposed CSI estimators. The proposed algorithm requires only limited CSI of the beamspace channel, namely the non-zero coefficients and their respective indices, which

¹The total coherence of a matrix $\tilde{\Phi}$ having G columns, denoted as $\mu^t(\tilde{\Phi})$, is defined as $\mu^t(\tilde{\Phi}) = \sum_{i=1}^G \sum_{j=1, j \neq i}^G |\tilde{\Phi}_i^H \tilde{\Phi}_j|^2$, where the quantities $\tilde{\Phi}_i$ and $\tilde{\Phi}_j$ represent the i th and j th columns, respectively, of the matrix $\tilde{\Phi}$.

substantially reduces the feedback required. Furthermore, in contrast to the existing hybrid transceiver designs [13], [15], [41], [42], the proposed hybrid transceiver design requires no iterations, and hence it is computationally efficient.

- 5) Our simulation results demonstrate the enhanced performance of our channel estimators, TPC and RC for various practical simulation parameters. In this context, this paper calculates the molecular absorption coefficient using the parameters obtained from the HITRAN database [43], which is suitable for the entire THz band, specifically for the higher end spanning 1 to 10 THz. On the other hand, most of the existing works employ models, which are only valid for the lower end around 0.1 to 0.3 THz.

C. Organization and Notation

The main focus of this work is on hybrid transceiver design relying on the BL-based estimated beamspace domain CSI. To achieve this, in Section-II, we begin with the THz MIMO system and channel model, which incorporates the specific molecular absorption and reflection losses arising in the THz regime. This is followed by developing its sparse beamspace domain representation and a novel frame-based channel estimation model in Section-III, which excites various angular modes of the THz MIMO channel. Furthermore, in order to improve the sparse CSI estimation performance, the *mutual coherence* of the equivalent sensing matrix has also been minimized in Section-III, which results in the optimal choice of the training precoders/combiners to be employed during channel estimation. Subsequently, the proposed BL and MBL-based sparse channel estimation schemes are developed in Section-IV, which is followed by the BCRLB for benchmarking their CSI estimation performance. Finally, based on the estimated CSI, the problem of designing the capacity-optimal hybrid precoder and MMSE-optimal hybrid combiner is addressed in Section-V. Our simulation results are presented in Section-VI, followed by our conclusions in Section-VII.

Notation: The notation $\text{floor}[a]$ represents the greatest integer, which is less than a , whereas $\text{rem}[a, b]$ denotes the remainder, when a is divided by b ; the i th element of the vector \mathbf{a} and (i, j) th element of the matrix \mathbf{A} are denoted by $\mathbf{a}(i)$ and $\mathbf{A}(i, j)$, respectively; \mathbf{I}_N denotes an identity matrix of size N ; $\text{vec}(\mathbf{A})$ vectorizes the columns of the matrix \mathbf{A} and $\text{vec}^{-1}(\mathbf{a})$ denotes the inverse vectorization operation; the Kronecker product of two matrices \mathbf{A} and \mathbf{B} is denoted by $\mathbf{A} \otimes \mathbf{B}$; the l_2 - and Frobenius-norm are represented by $\|\cdot\|_2$ and $\|\cdot\|_F$, respectively.

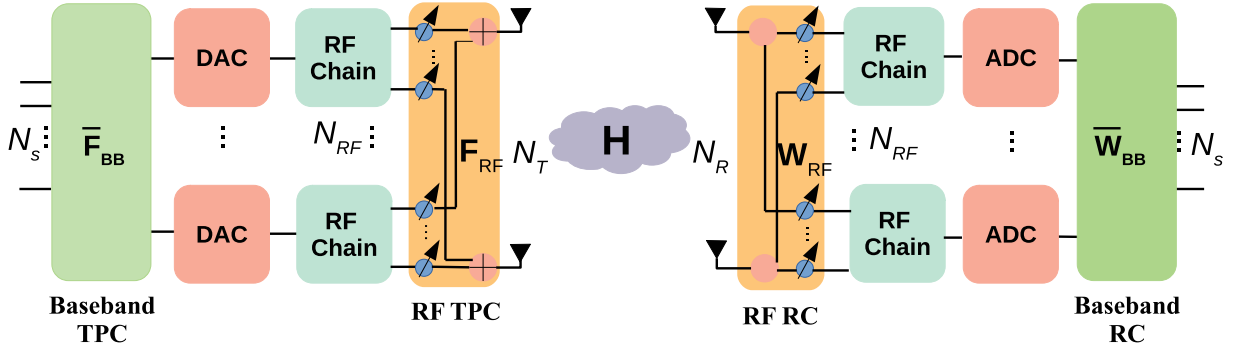


Fig. 1: Block diagram of a THz hybrid MIMO system.

II. THZ MIMO SYSTEM AND CHANNEL MODEL

The schematic of our THz hybrid MIMO system is portrayed in Fig. 1, where N_T and N_R denote the number of transmit antennas (TAs) and receive antennas (RAs), respectively, whereas N_{RF} denotes the number of RF chains. Furthermore, N_S is the number of data streams, where $N_S \leq N_{RF}$, while $N_{RF} \ll \min(N_T, N_R)$ [5], [27]. The transmitter is composed of two major blocks, the digital baseband TPC $\bar{\mathbf{F}}_{BB} \in \mathbb{C}^{N_{RF} \times N_S}$ and the analog RF TPC $\bar{\mathbf{F}}_{RF} \in \mathbb{C}^{N_T \times N_{RF}}$. At the receiver side, $\bar{\mathbf{W}}_{RF} \in \mathbb{C}^{N_R \times N_{RF}}$ denotes the RF RC, whereas $\bar{\mathbf{W}}_{BB} \in \mathbb{C}^{N_{RF} \times N_S}$ represents the baseband RC. As described in [5], [27], the analog RF TPC $\bar{\mathbf{F}}_{RF}$ and RC $\bar{\mathbf{W}}_{RF}$ are comprised of APSs. Hence, for simplicity, these are constrained as $|\bar{\mathbf{F}}_{RF}(i, j)| = \frac{1}{\sqrt{N_T}}$, $|\bar{\mathbf{W}}_{RF}(i, j)| = \frac{1}{\sqrt{N_R}}$, $\forall i, j$. Thus, the baseband system model of our THz MIMO system is given by

$$\bar{\mathbf{y}} = \bar{\mathbf{W}}_{BB}^H \bar{\mathbf{W}}_{RF}^H \mathbf{H} \bar{\mathbf{F}}_{RF} \bar{\mathbf{F}}_{BB} \bar{\mathbf{x}} + \bar{\mathbf{W}}_{BB}^H \bar{\mathbf{W}}_{RF}^H \bar{\mathbf{v}}, \quad (1)$$

where $\bar{\mathbf{y}} \in \mathbb{C}^{N_S \times 1}$ is the signal vector received at the output of the baseband RC, $\bar{\mathbf{x}} \in \mathbb{C}^{N_S \times 1}$ represents the transmit baseband signal vector at the input of the baseband TPC, whereas the quantity $\bar{\mathbf{v}} \in \mathbb{C}^{N_R \times 1}$ is the complex additive white Gaussian noise (AWGN) at the receiver having the distribution of $\mathcal{CN}(\mathbf{0}_{N_R \times 1}, \sigma_v^2 \mathbf{I}_{N_R})$. The matrix $\mathbf{H} \in \mathbb{C}^{N_R \times N_T}$ in (1) represents the baseband equivalent of the THz MIMO channel, whose relevant model is described next.

A. THz MIMO Channel Model

As described in [11], the THz MIMO channel can be modeled as the aggregation of a line-of-sight (LoS) and a few NLoS components. The LoS propagation results in a direct path between the BS and the UE, whereas the NLoS propagation results in some indirect multipath rays after

reflection from the various scatterers present in the environment. Thus, the THz MIMO channel \mathbf{H} , which is a function of the operating frequency f and distance d , can be expressed as

$$\mathbf{H}(f, d) = \mathbf{H}_{\text{LoS}}(f, d) + \mathbf{H}_{\text{NLoS}}(f, d), \quad (2)$$

where the LoS and NLoS components are given by

$$\mathbf{H}_{\text{LoS}}(f, d) = \sqrt{\frac{N_T N_R}{N_{\text{ray}}}} \sum_{j=1}^{N_{\text{ray}}} \alpha_{\text{L},j}(f, d) G_t^a G_r^a \mathbf{a}_r(\phi_{\text{L},j}^r) \mathbf{a}_t^H(\phi_{\text{L},j}^t), \quad (3)$$

$$\mathbf{H}_{\text{NLoS}}(f, d) = \sqrt{\frac{N_T N_R}{N_{\text{NLoS}} N_{\text{ray}}}} \sum_{i=1}^{N_{\text{NLoS}}} \sum_{j=1}^{N_{\text{ray}}} \alpha_{i,j}(f, d) G_t^a G_r^a \mathbf{a}_r(\phi_{i,j}^r) \mathbf{a}_t^H(\phi_{i,j}^t). \quad (4)$$

Here, the quantities $\alpha_{\text{L},j}(f, d)$ and $\alpha_{i,j}(f, d)$ represent the complex-valued path-gains of the LoS and NLoS components, respectively, N_{NLoS} denotes the number of NLoS multipath components, whereas N_{ray} signifies the number of diffused-rays in each multipath component. Furthermore, G_t^a and G_r^a represent the TA and RA gains, respectively. The quantities $\phi_{\text{L},j}^r$ and $\phi_{\text{L},j}^t$ denote the AoA and AoD of the j th ray in the LoS multipath component, respectively, whereas $\phi_{i,j}^r$ and $\phi_{i,j}^t$ represent the AoA and AoD of the j th diffuse-ray in the i th NLoS multipath component. The vectors $\mathbf{a}_r(\phi^r) \in \mathbb{C}^{N_R \times 1}$ and $\mathbf{a}_t(\phi^t) \in \mathbb{C}^{N_T \times 1}$ denote the array response vectors of the uniform linear array (ULA) corresponding to the AoA ϕ^r at the receiver and AoD ϕ^t at the transmitter, respectively. These are defined as

$$\mathbf{a}_r(\phi^r) = \frac{1}{\sqrt{N_R}} \left[1, e^{-j\frac{2\pi}{\lambda} d_r \cos(\phi^r)}, \dots, e^{-j\frac{2\pi}{\lambda} (N_R-1) d_r \cos(\phi^r)} \right]^T, \quad (5)$$

$$\mathbf{a}_t(\phi^t) = \frac{1}{\sqrt{N_T}} \left[1, e^{-j\frac{2\pi}{\lambda} d_t \cos(\phi^t)}, \dots, e^{-j\frac{2\pi}{\lambda} (N_T-1) d_t \cos(\phi^t)} \right]^T, \quad (6)$$

where d_r and d_t represent the antenna-spacings at the receiver and transmitter, respectively, and λ denotes the operating wavelength.

Let the complex path-gain $\alpha(f, d)$ be expressed as $\alpha(f, d) = |\alpha(f, d)|e^{j\psi}$, where $|\alpha(f, d)|$ is the magnitude of the complex path-gain and ψ is the associated independent phase shift. According to [4], [11], the magnitude of the LoS path gain $|\alpha_{\text{L},j}(f, d)|$ can be modeled as

$$|\alpha_{\text{L},j}(f, d)|^2 = L_{\text{spread}}(f, d) L_{\text{abs}}(f, d), \quad (7)$$

where $L_{\text{spread}}(f, d)$ and $L_{\text{abs}}(f, d)$ represent the spreading (or the free-space) and molecular absorption losses respectively, which are given by

$$L_{\text{abs}}(f, d) = e^{-k_{\text{abs}}(f)d}, \quad L_{\text{spread}}(f, d) = \left(\frac{c}{4\pi f d} \right)^2. \quad (8)$$

Here, c denotes the speed of light in vacuum and $k_{\text{abs}}(f)$ is the molecular absorption coefficient. Similarly, for the j th diffuse-ray of the i th NLoS multipath component, the magnitude of the complex path-gain can be expressed as [5], [11]

$$|\alpha_{i,j}(f, d)|^2 = \Gamma_{i,j}^2(f) L_{\text{spread}}(f, d) L_{\text{abs}}(f, d), \quad (9)$$

where $\Gamma_{i,j}(f)$ denotes the first-order reflection coefficient of the j th diffuse-ray of the i th NLoS component. For higher-order reflections, the equivalent reflection coefficient is equal to the product of individual reflection coefficients of the respective scattering media. Further details on the calculation of the absorption coefficient $k_{\text{abs}}(f)$ and the reflection coefficient $\Gamma_{i,j}(f)$ are given in the subsequent subsections.

B. Calculation of the Reflection Coefficient $\Gamma(f)$

Due to the small wavelength of the THz signal, the reflection coefficient $\Gamma(f)$ is an important parameter to be taken into account while evaluating the losses of the NLoS components [11], [44]. This is in turn defined in terms of the Fresnel reflection coefficient (γ) and the Rayleigh roughness factor (ϱ), as $\Gamma(f) = \gamma(f)\varrho(f)$, where the coefficients $\gamma(f)$ and $\varrho(f)$ are given by:

$$\gamma(f) = \frac{Z(f) \cos(\theta_{\text{in}}) - Z_0 \cos(\theta_{\text{ref}})}{Z(f) \cos(\theta_{\text{in}}) + Z_0 \cos(\theta_{\text{ref}})} \quad \text{and} \quad \varrho(f) = e^{-\frac{1}{2} \left(\frac{4\pi f \sigma \cos(\theta_{\text{in}})}{c} \right)^2}. \quad (10)$$

In the above expressions, θ_{in} denotes the angle of incidence, while θ_{ref} represents the angle of refraction, which obeys $\theta_{\text{ref}} = \sin^{-1} \left(\sin(\theta_{\text{in}}) \frac{Z(f)}{Z_0} \right)$. The quantity $Z(f)$ denotes the wave impedance of the reflecting medium, whereas $Z_0 = 377 \Omega$ represents the wave impedance of the free space and σ in (10) denotes the standard deviation of the reflecting surface's roughness.

C. Absorption Coefficient $k_{\text{abs}}(f)$ [4]

As described in [4], the absorption coefficient $k_{\text{abs}}(f)$ of the propagation medium at frequency f can be evaluated as

$$k_{\text{abs}}(f) = \sum_{i,g} k_{\text{abs}}^{i,g}(f), \quad (11)$$

where, $k_{\text{abs}}^{i,g}$ denotes the absorption coefficient of the i th isotopologue² of the g th gas. The quantity $k_{\text{abs}}^{i,g}(f)$ can be mathematically defined as

$$k_{\text{abs}}^{i,g}(f) = \left(\frac{p}{p_0} \right) \left(\frac{T_{\text{STP}}}{T} \right) Q^{i,g} \sigma^{i,g}(f), \quad (12)$$

²Molecules, which only differ from others in their isotopic composition, are termed as isotopologues of each other.

where p and T denote the system pressure and temperature, respectively, while T_{STP} and p_0 represent the temperature at standard pressure and reference pressure, respectively. The quantity $\sigma^{i,g}$ denotes the absorption cross-section of the i th isotopologue of the g th gas, defined as $\sigma^{i,g}(f) = S^{i,g}G^{i,g}(f)$, and $Q^{i,g}$ is the molecular volumetric density, defined as $Q^{i,g} = \left(\frac{p}{RT}\right)q^{i,g}N_A$. Here, R denotes the gas constant and N_A represents Avogadro's number. The quantities $q^{i,g}$ and $S^{i,g}$ signify the mixing ratio and the line intensity, respectively, of the i th isotopologue of the g th gas, which can be directly obtained from the HITRAN database [10]. The quantity $G^{i,g}(f)$ is the spectral line shape, defined as

$$G^{i,g}(f) = \left(\frac{f}{f_c^{i,g}}\right) \frac{\tanh\left(\frac{cfh}{2k_B T}\right)}{\tanh\left(\frac{cf_c^{i,g}h}{2k_B T}\right)} F^{i,g}(f), \quad (13)$$

where k_B denotes the Boltzmann constant, h represents the Planck constant and $F^{i,g}(f)$ is the Van Vleck-Weisskopf line shape [45], which is evaluated as follows

$$F^{i,g}(f) = \frac{100cf\alpha_L^{i,g}}{\pi f_c^{i,g}} \sum_{n=1}^2 \frac{1}{(f + (-1)^n f_c^{i,g})^2 + (\alpha_L^{i,g})^2}. \quad (14)$$

The quantities $f_c^{i,g}$ and $\alpha_L^{i,g}$ obey:

$$f_c^{i,g} = f_{c0}^{i,g} + \delta^{i,g} \frac{p}{p_0} \text{ and } \alpha_L^{i,g} = [(1 - q^{i,g})\alpha_0^{\text{air}} + q^{i,g}\alpha_0^{i,g}] \left(\frac{p}{p_0}\right) \left(\frac{T_0}{T}\right)^\gamma, \quad (15)$$

where $f_{c0}^{i,g}$ and $\delta^{i,g}$ denote the zero-pressure resonance frequency and linear pressure shift, respectively, which are also obtained from the HITRAN database. In (15), α_0^{air} and $\alpha_0^{i,g}$ represent the broadening coefficient of the air and of the i th isotopologue of the g th gas, respectively, whereas γ denotes the temperature broadening coefficient, all of which can be directly obtained from the HITRAN database, and the quantity T_0 denotes the reference temperature. The parameters involved in the calculation of molecular absorption coefficient $k_{\text{abs}}(f)$, their units and the values of various constants are summarized in Table-I of [4]. Furthermore, the HITRAN database is accessible online from [43].

From the channel model presented in this section, it can be readily observed that the THz MIMO channel is significantly different from its mmWave counterpart. First of all, note that the THz MIMO channel is highly dependent on the carrier frequency f and distance d , not just due to the free-space loss $L_{\text{spread}}(f, d)$, but more importantly due to the nature of molecular absorption loss $L_{\text{abs}}(f, d) = e^{-k_{\text{abs}}(f)d}$, where the absorption coefficient $k_{\text{abs}}(f)$ is highly dependent on the molecular composition of the propagation medium, system pressure, temperature and the

operating frequency. In fact, as evaluated in [4], even the water vapor molecules present in a standard medium lead to a significant loss, which affects the overall system performance in the THz band. By contrast, in the mmWave band, these atmospheric losses only become significant in the presence of raindrops/ fog. Due to this, THz signals experience severe propagation losses beyond a few meters. Furthermore, due to the extremely short wavelength of THz signals, the indoor surfaces, which can be regarded as smooth in the comparatively lower mmWave band, now appear rough in the THz regime [11]. Hence, it can be observed from (7) and (9) that the complex-valued path gains $\alpha_{L,j}(f, d)$ and $\alpha_{i,j}(f, d)$ in the THz band for the LoS and NLoS components, respectively, differ significantly due to their increased higher-order reflection losses. Additionally, due to the large number of antennas, the THz MIMO channel becomes highly directional and more sparse in nature in comparison to its mmWave counterpart. It has also been verified in [4] and also in our simulation results that at certain frequencies, the molecular absorption is very high, which reduces the total bandwidth to just a few transmission windows. Hence, the molecular absorption plays a critical role in deciding the operating frequency and bandwidth. The next section describes the channel estimation model proposed for our THz MIMO systems. For ease of notation, we drop the quantities (f, d) from the THz MIMO channel representation in the subsequent sections, since these parameters are fixed for the channel under consideration.

III. THZ MIMO CHANNEL ESTIMATION MODEL

Consider the transmission of $N_F = \frac{N_T}{N_{RF}}$ training frames and M_T training vectors, where $M_T < N_T$. This implies that $\frac{M_T}{N_F}$ training vectors are transmitted in each frame. Let $\mathbf{F}_{RF,i} \in \mathbb{C}^{N_T \times N_{RF}}$ represent the RF training TPC and $\mathbf{X}_{p,i} \in \mathbb{C}^{N_{RF} \times \frac{M_T}{N_F}}$ denote the pilot matrix corresponding to the i th training frame. The received pilot matrix $\tilde{\mathbf{Y}}_i \in \mathbb{C}^{N_R \times \frac{M_T}{N_F}}$ can be represented as

$$\tilde{\mathbf{Y}}_i = \mathbf{H}\mathbf{F}_{RF,i}\mathbf{X}_{p,i} + \tilde{\mathbf{V}}_i, \quad (16)$$

where $\tilde{\mathbf{V}}_i \in \mathbb{C}^{N_R \times \frac{M_T}{N_F}}$ denotes the noise matrix having independent and identically distributed (i.i.d.) elements obeying $\mathcal{CN}(0, \sigma_v^2)$. Upon concatenating $\tilde{\mathbf{Y}}_i$ for $1 \leq i \leq N_F$, as $\tilde{\mathbf{Y}} = [\tilde{\mathbf{Y}}_1, \tilde{\mathbf{Y}}_2, \dots, \tilde{\mathbf{Y}}_{N_F}] \in \mathbb{C}^{N_R \times M_T}$, one can model the received pilot matrix as

$$\tilde{\mathbf{Y}} = \mathbf{H}\mathbf{F}_{RF}\mathbf{X}_p + \tilde{\mathbf{V}}, \quad (17)$$

where the various quantities are defined as $\mathbf{F}_{RF} = [\mathbf{F}_{RF,1}, \mathbf{F}_{RF,2}, \dots, \mathbf{F}_{RF,N_F}] \in \mathbb{C}^{N_T \times N_T}$, $\tilde{\mathbf{V}} = [\tilde{\mathbf{V}}_1, \tilde{\mathbf{V}}_2, \dots, \tilde{\mathbf{V}}_{N_F}] \in \mathbb{C}^{N_R \times M_T}$ and

$$\mathbf{X}_p = \text{blkdiag}(\mathbf{X}_{p,1}, \mathbf{X}_{p,2}, \dots, \mathbf{X}_{p,N_F}) \in \mathbb{C}^{N_T \times M_T}, \quad (18)$$

Similarly, let $N_C = \frac{N_R}{N_{\text{RF}}}$ represent the number of combining-steps, whereas M_R denote the number of combining vectors. In each combining-step, we combine the pilot output $\tilde{\mathbf{Y}}$ using $\frac{M_R}{N_C}$ combining vectors in the baseband, where $M_R < N_R$. Let $\mathbf{W}_{\text{RF},j} \in \mathbb{C}^{N_R \times N_{\text{RF}}}$ denote the RF RC and $\mathbf{W}_{\text{BB},j} \in \mathbb{C}^{N_{\text{RF}} \times \frac{M_R}{N_C}}$ represent the baseband RC of the j th combining step. The received pilot matrix $\mathbf{Y}_j \in \mathbb{C}^{\frac{M_R}{N_C} \times M_T}$ at the output of the j th baseband RC is obtained as $\mathbf{Y}_j = \mathbf{W}_{\text{BB},j}^H \mathbf{W}_{\text{RF},j}^H \tilde{\mathbf{Y}}$. Let $\mathbf{Y} = [\mathbf{Y}_1^T, \mathbf{Y}_2^T, \dots, \mathbf{Y}_{N_C}^T]^T \in \mathbb{C}^{M_R \times M_T}$ represent the stacked received pilot matrices $\mathbf{Y}_j, 1 \leq j \leq N_C$. The end-to-end model can be succinctly represented as

$$\mathbf{Y} = \mathbf{W}_{\text{BB}}^H \mathbf{W}_{\text{RF}}^H \mathbf{H} \mathbf{F}_{\text{RF}} \mathbf{X}_p + \mathbf{V}, \quad (19)$$

where the various quantities have the following expressions: $\mathbf{W}_{\text{RF}} = [\mathbf{W}_{\text{RF},1}, \mathbf{W}_{\text{RF},2}, \dots, \mathbf{W}_{\text{RF},N_C}] \in \mathbb{C}^{N_R \times N_R}$, $\mathbf{V} = \mathbf{W}_{\text{BB}}^H \mathbf{W}_{\text{RF}}^H \tilde{\mathbf{V}} \in \mathbb{C}^{M_R \times M_T}$ and

$$\mathbf{W}_{\text{BB}} = \text{blkdiag}(\mathbf{W}_{\text{BB},1}, \dots, \mathbf{W}_{\text{BB},N_C}) \in \mathbb{C}^{N_R \times M_R}. \quad (20)$$

One can now exploit the properties of the matrix Kronecker product [46] to arrive at the following THz MIMO channel estimation model

$$\mathbf{y} = \Phi \mathbf{h} + \mathbf{v}, \quad (21)$$

where $\mathbf{y} = \text{vec}(\mathbf{Y}) \in \mathbb{C}^{M_T M_R \times 1}$ represents the received pilot vector and $\mathbf{v} = \text{vec}(\mathbf{V}) \in \mathbb{C}^{M_T M_R \times 1}$ denotes the noise vector. The quantity $\mathbf{h} = \text{vec}(\mathbf{H}) \in \mathbb{C}^{N_T N_R \times 1}$ is the equivalent THz MIMO channel vector and the matrix $\Phi \in \mathbb{C}^{M_T M_R \times N_T N_R}$ represents the *sensing matrix* obeying $\Phi = [(\mathbf{X}_p^T \mathbf{F}_{\text{RF}}^T) \otimes (\mathbf{W}_{\text{BB}}^H \mathbf{W}_{\text{RF}}^H)]$. Finally, the noise covariance matrix $\mathbf{R}_v \in \mathbb{C}^{M_T M_R \times M_T M_R}$, defined as $\mathbf{R}_v = \mathbb{E}\{\mathbf{v}\mathbf{v}^H\}$, is given as $\mathbf{R}_v = \sigma_v^2 [\mathbf{I}_{M_T} \otimes (\mathbf{W}_{\text{BB}}^H \mathbf{W}_{\text{RF}}^H \mathbf{W}_{\text{RF}} \mathbf{W}_{\text{BB}})]$. At this point, it can be noted that the expressions for the conventional LS and MMSE estimates of the THz MIMO channel vector \mathbf{h} can be readily derived from the simplified model in (21), as

$$\hat{\mathbf{h}}^{\text{LS}} = (\Phi)^\dagger \mathbf{y} \quad \text{and} \quad \hat{\mathbf{h}}^{\text{MMSE}} = (\mathbf{R}_h^{-1} + \Phi^H \mathbf{R}_v^{-1} \Phi)^{-1} \Phi^H \mathbf{y}, \quad (22)$$

where $\mathbf{R}_h = \mathbb{E}[\mathbf{h}\mathbf{h}^H] \in \mathbb{C}^{N_T N_R \times N_T N_R}$ represents the channel's covariance matrix. However, a significant drawback of these conventional estimation techniques is that they require an over-determined system, i.e., $M_T M_R \geq N_T N_R$, for reliable channel estimation. This results in unsustainably high training overheads due to the high number of antennas. Thus, conventional channel estimation techniques are inefficient for such systems. Furthermore, as described in [5], [11], the THz MIMO channel exhibits *angular-sparsity*, which is not exploited by these conventional techniques. Leveraging the sparsity of the THz MIMO channel can lead to significantly improved

channel estimation performance as well as bandwidth-efficiency, specifically where we have the ‘ill-posed’ THz MIMO channel estimation scenario of $M_T M_R \ll N_T N_R$. Thus, the next subsection derives a sparse channel estimation model for THz MIMO systems.

A. Sparse THz MIMO Channel Estimation Model

Let G_T and G_R signify the angular grid-sizes obeying $(G_T, G_R) \geq \max(N_T, N_R)$. The angular grids Φ_T and Φ_R for the AoD and AoA, respectively, are given as follows, which are constructed by assuming the directional-cosines $\cos(\phi_i)$ to be uniformly spaced between -1 to 1 :

$$\Phi_T = \left\{ \phi_i : \cos(\phi_i) = \frac{2}{G_T}(i-1) - 1, 1 \leq i \leq G_T \right\}, \quad (23)$$

$$\Phi_R = \left\{ \phi_j : \cos(\phi_j) = \frac{2}{G_R}(j-1) - 1, 1 \leq j \leq G_R \right\}. \quad (24)$$

Let $\mathbf{A}_R(\Phi_R) \in \mathbb{C}^{N_R \times G_R}$ and $\mathbf{A}_T(\Phi_T) \in \mathbb{C}^{N_T \times G_T}$ represent the dictionary matrices of the array responses constructed using the angular-grids Φ_R and Φ_T as follows

$$\mathbf{A}_R(\Phi_R) = [\mathbf{a}_r(\phi_1), \mathbf{a}_r(\phi_2), \dots, \mathbf{a}_r(\phi_{G_R})], \quad \mathbf{A}_T(\Phi_T) = [\mathbf{a}_t(\phi_1), \mathbf{a}_t(\phi_2), \dots, \mathbf{a}_t(\phi_{G_T})]. \quad (25)$$

Owing to the choice of grid angles considered in (23) and (24), the matrices $\mathbf{A}_R(\Phi_R)$ and $\mathbf{A}_T(\Phi_T)$ are semi-unitary, i.e., they satisfy

$$\mathbf{A}_i(\Phi_i) \mathbf{A}_i^H(\Phi_i) = \frac{G_i}{N_i} \mathbf{I}_{N_i}, \quad i \in \{R, T\}. \quad (26)$$

Using the above quantities, an equivalent angular-domain beamspace representation [6], [16] of the THz MIMO channel \mathbf{H} (c.f. (2)) can be obtained as

$$\mathbf{H} \simeq \mathbf{A}_R(\Phi_R) \mathbf{H}_b \mathbf{A}_T^H(\Phi_T), \quad (27)$$

where $\mathbf{H}_b \in \mathbb{C}^{G_R \times G_T}$ signifies the beamspace domain channel matrix. Note that when the grid sizes G_R and G_T are large, i.e., the quantization of AoA/ AoD grids is fine enough, the above approximate relationship holds with equality. Due to high free-space loss, as well as reflection and molecular absorption losses in a THz system, the number of multipath components is significantly lower [5], [11], [24]. Furthermore, the THz MIMO channel comprises only a few highly-directional beams, which results in an angularly-sparse multipath channel. Hence, only a few active AoA/ AoD pairs exist in the channel, which makes the beamspace channel matrix \mathbf{H}_b sparse in nature.

Once again, upon exploiting the properties of the matrix Kronecker product in (27), one obtains

$$\mathbf{h} = \text{vec}(\mathbf{H}) = [\mathbf{A}_T^*(\Phi_T) \otimes \mathbf{A}_R(\Phi_R)] \mathbf{h}_b, \quad (28)$$

where $\mathbf{h}_b = \text{vec}(\mathbf{H}_b) \in \mathbb{C}^{G_R G_T \times 1}$. Finally, the sparse CSI estimation model of the THz MIMO system can be obtained via substitution of (28) into (21), yielding

$$\mathbf{y} = \tilde{\Phi} \mathbf{h}_b + \mathbf{v}, \quad (29)$$

where $\tilde{\Phi} = \Phi \Psi \in \mathbb{C}^{M_T M_R \times G_R G_T}$ represents the equivalent sensing matrix, whereas $\Psi = [\mathbf{A}_T^*(\Phi_T) \otimes \mathbf{A}_R(\Phi_R)] \in \mathbb{C}^{N_R N_T \times G_R G_T}$ represents the *sparsifying-dictionary*. Alternatively, one can express the equivalent sensing matrix $\tilde{\Phi}$ as

$$\tilde{\Phi} = [(\mathbf{X}_p^T \mathbf{F}_{RF}^T \mathbf{A}_T^*(\Phi_T)) \otimes (\mathbf{W}_{BB}^H \mathbf{W}_{RF}^H \mathbf{A}_R(\Phi_R))]. \quad (30)$$

It can be readily observed that the equivalent sensing matrix $\tilde{\Phi}$ depends on the choice of the RF TPC \mathbf{F}_{RF} , of the RF RC \mathbf{W}_{RF} , of the baseband RC \mathbf{W}_{BB} and of the pilot matrix \mathbf{X}_p employed for estimating the channel. Therefore, minimizing the total coherence [38], [39] of the matrix $\tilde{\Phi}$ can lead to significantly improved sparse signal estimation. We now derive the optimal pilot matrix \mathbf{X}_p and the baseband RC \mathbf{W}_{BB} , which achieve this.

Lemma 1. *Let us set the RF TPC and RC to the normalized discrete Fourier transform (DFT) matrices as follows: $\mathbf{F}_{RF} \mathbf{F}_{RF}^H = \mathbf{F}_{RF}^H \mathbf{F}_{RF} = \mathbf{I}_{N_T}$ and $\mathbf{W}_{RF} \mathbf{W}_{RF}^H = \mathbf{W}_{RF}^H \mathbf{W}_{RF} = \mathbf{I}_{N_R}$. Then the i th diagonal block $\mathbf{X}_{p,i}$, $1 \leq i \leq N_F$, of the pilot matrix \mathbf{X}_p defined in (18), and j th diagonal block $\mathbf{W}_{BB,j}$, $1 \leq j \leq N_C$, of the baseband RC \mathbf{W}_{BB} defined in (20), may be formulated as*

$$\mathbf{X}_{p,i} = \mathbf{U} \begin{bmatrix} \mathbf{I}_{\frac{M_T}{N_F}} & \mathbf{0}_{\frac{M_T}{N_F} \times N_{RF} - \frac{M_T}{N_F}} \end{bmatrix}^T \mathbf{V}_1^H \quad \text{and} \quad \mathbf{W}_{BB,j} = \mathbf{U} \begin{bmatrix} \mathbf{I}_{\frac{M_R}{N_C}} & \mathbf{0}_{\frac{M_R}{N_C} \times N_{RF} - \frac{M_R}{N_C}} \end{bmatrix}^T \mathbf{V}_2^H, \quad (31)$$

for which the total coherence $\mu^t(\tilde{\Phi})$ of the equivalent dictionary matrix $\tilde{\Phi}$ is minimized, where the matrices \mathbf{U} , \mathbf{V}_1 and \mathbf{V}_2 are arbitrary unitary matrices of size $N_{RF} \times N_{RF}$, $\frac{M_T}{N_F} \times \frac{M_T}{N_F}$ and $\frac{M_R}{N_C} \times \frac{M_R}{N_C}$, respectively.

Proof. Given in Appendix A. □

The next subsection develops an OMP-based procedure for acquiring a sparse estimate of the THz MIMO channel exploiting the model of (29).

Algorithm 1 OMP-based sparse channel estimation for THz MIMO systems

Input: Equivalent sensing matrix $\tilde{\Phi}$, pilot output \mathbf{y} , array response dictionary matrices $\mathbf{A}_R(\Phi_R)$ and $\mathbf{A}_T(\Phi_T)$, stopping parameter ϵ_t

Initialization: Index set $\mathcal{I} = []$, $\tilde{\Phi}^{\mathcal{I}} = []$, residue vectors $\mathbf{r}_{-1} = \mathbf{0}_{M_T M_R \times 1}$, $\mathbf{r}_0 = \mathbf{y}$, $\hat{\mathbf{h}}_{b, \text{OMP}} = \mathbf{0}_{G_R G_T \times 1}$, counter $i = 0$

while ($|\|\mathbf{r}_{i-1}\|_2^2 - \|\mathbf{r}_i\|_2^2| \geq \epsilon_t$) **do**

- 1) $i \leftarrow i + 1$
- 2) $j = \arg \max_{k=1, \dots, G_T G_R} |\mathbf{r}_{i-1}^H \tilde{\Phi}(:, k)|$
- 3) $\mathcal{I} = \mathcal{I} \cup j$
- 4) $\tilde{\Phi}^{\mathcal{I}} = \tilde{\Phi}(:, \mathcal{I})$
- 5) $\hat{\mathbf{h}}_{\text{LS}}^i = (\tilde{\Phi}^{\mathcal{I}})^\dagger \mathbf{y}$
- 6) $\mathbf{r}_i = \mathbf{y} - \tilde{\Phi}^{\mathcal{I}} \hat{\mathbf{h}}_{\text{LS}}^i$

end while

$$\hat{\mathbf{h}}_{b, \text{OMP}}(\mathcal{I}) = \hat{\mathbf{h}}_{\text{LS}}^i$$

Output: $\hat{\mathbf{H}}_{\text{OMP}} = \mathbf{A}_R(\Phi_R) \text{vec}^{-1} \left(\hat{\mathbf{h}}_{b, \text{OMP}} \right) \mathbf{A}_T^H(\Phi_T)$

B. OMP-Based Sparse Channel Estimation in THz Hybrid MIMO Systems

The OMP-based sparse channel estimation technique is summarized in Algorithm 1 and its key steps are described next. Step-2 of each iteration identifies the specific column of the sensing matrix $\tilde{\Phi}$ that is maximally correlated with the residue \mathbf{r}_{i-1} obtained in iteration $i - 1$. Step-3 updates the index-set \mathcal{I} by including the index j obtained in Step-2. Subsequently, Step-4 determines the submatrix $\tilde{\Phi}^{\mathcal{I}}$ of the sensing matrix $\tilde{\Phi}$ using the specific columns, which are indexed by the set \mathcal{I} . Step-5 obtains the intermediate LS solution $\hat{\mathbf{h}}_{\text{LS}}^i$, while the associated residue vector \mathbf{r}_i is computed using $\tilde{\Phi}^{\mathcal{I}}$ in Step-6. These steps are repeated iteratively until the difference between the subsequent residuals becomes sufficiently small, i.e., $|\|\mathbf{r}_{i-1}\|_2^2 - \|\mathbf{r}_i\|_2^2| < \epsilon_t$, where ϵ_t is a suitably chosen threshold. Finally, the OMP-based estimate $\hat{\mathbf{H}}_{\text{OMP}}$ of the THz MIMO channel using its beamspace estimate $\hat{\mathbf{h}}_{b, \text{OMP}}$ is determined as $\hat{\mathbf{H}}_{\text{OMP}} = \mathbf{A}_R(\Phi_R) \text{vec}^{-1} \left(\hat{\mathbf{h}}_{b, \text{OMP}} \right) \mathbf{A}_T^H(\Phi_T)$. The key benefits of the proposed OMP algorithm are its sparsity inducing nature and low computational cost. However, note that the choice of the stopping parameter ϵ_t plays a vital role in defining the convergence behavior of the OMP algorithm, which renders the performance uncertain. Furthermore, this technique is susceptible to error propagation due to its greedy

nature, since an errant selection of the index in a particular iteration cannot be corrected in the subsequent iterations. In view of these shortcomings of the OMP-based approach, the next subsection develops an efficient BL-based framework, which leads to a significantly improved estimation accuracy of the THz MIMO channel.

IV. BL-BASED SPARSE CHANNEL ESTIMATION IN THZ MIMO SYSTEMS

The proposed BL-based sparse channel estimation technique relies on the Bayesian philosophy, which is especially well-suited for an under-determined system, where $M_T M_R \ll G_T G_R$. A brief outline of this procedure is as follows. The BL procedure commences by assigning a parameterized Gaussian prior $f(\mathbf{h}_b; \mathbf{\Gamma})$ to the sparse beamspace CSI vector \mathbf{h}_b . The associated hyperparameter matrix $\mathbf{\Gamma}$ is subsequently estimated by maximizing the Bayesian evidence $f(\mathbf{y}; \mathbf{\Gamma})$. Finally, the MMSE estimate of the beamspace channel is obtained using the estimated hyperparameter matrix $\hat{\mathbf{\Gamma}}$, which leads to an improved sparse channel estimate. The various steps are described in detail below.

Consider the parameterized Gaussian prior assigned to \mathbf{h}_b as shown below [47]

$$f(\mathbf{h}_b; \mathbf{\Gamma}) = \prod_{i=1}^{G_R G_T} (\pi \gamma_i)^{-1} \exp\left(-\frac{|\mathbf{h}_b(i)|^2}{\gamma_i}\right), \quad (32)$$

where the matrix $\mathbf{\Gamma} = \text{diag}(\gamma_1, \gamma_2, \dots, \gamma_{G_R G_T}) \in \mathbb{R}^{G_R G_T \times G_R G_T}$ comprises the hyperparameters γ_i , $1 \leq i \leq G_R G_T$. Note that the MMSE estimate $\hat{\mathbf{h}}_b$ corresponding to the sparse estimation model in (29) is given by [48]

$$\hat{\mathbf{h}}_b = \left(\tilde{\mathbf{\Phi}}^H \mathbf{R}_v^{-1} \tilde{\mathbf{\Phi}} + \mathbf{\Gamma}^{-1}\right)^{-1} \tilde{\mathbf{\Phi}}^H \mathbf{R}_v^{-1} \mathbf{y}, \quad (33)$$

which can be readily seen to depend on the hyperparameter matrix $\mathbf{\Gamma}$. Therefore, the estimation of $\mathbf{\Gamma}$ holds the key for eventually arriving at a reliable sparse estimate of the beamspace channel vector \mathbf{h}_b . In order to achieve this, consider the log-likelihood function $\log[f(\mathbf{y}; \mathbf{\Gamma})]$ of the hyperparameter matrix $\mathbf{\Gamma}$, which can be formulated as $\log[f(\mathbf{y}; \mathbf{\Gamma})] = c_1 - \log[\det(\mathbf{R}_y)] - \mathbf{y}^H \mathbf{R}_y^{-1} \mathbf{y}$, where we have $c_1 = -M_T M_R \log(\pi)$ and the matrix $\mathbf{R}_y = \mathbf{R}_v + \tilde{\mathbf{\Phi}} \mathbf{\Gamma} \tilde{\mathbf{\Phi}}^H \in \mathbb{C}^{M_T M_R \times M_T M_R}$ represents the covariance matrix of the pilot output \mathbf{y} . It follows from [47] that maximization of the log-likelihood $\log[f(\mathbf{y}; \mathbf{\Gamma})]$ with respect to $\mathbf{\Gamma}$ is non-concave, which renders its direct maximization intractable. Therefore, in such cases, the Expectation-Maximization (EM) technique is eminently suited for iterative maximization of the log-likelihood function, with guaranteed convergence to a local optimum [48]. Let $\hat{\gamma}_i^{(j-1)}$ denote the estimate of the i th hyperparameter

obtained from the EM iteration $(j - 1)$ and let $\widehat{\mathbf{\Gamma}}^{(j-1)}$ denote the hyperparameter matrix defined as $\widehat{\mathbf{\Gamma}}^{(j-1)} = \text{diag} \left(\widehat{\gamma}_1^{(j-1)}, \widehat{\gamma}_2^{(j-1)}, \dots, \widehat{\gamma}_{G_R G_T}^{(j-1)} \right)$. The procedure of updating the estimate $\widehat{\mathbf{\Gamma}}^{(j)}$ in the j th EM-iteration is described in Lemma 2 below.

Lemma 2. *Given the i th hyperparameter $\widehat{\gamma}_i^{(j-1)}$, the update $\widehat{\gamma}_i^{(j)}$ in the j th EM-iteration, which maximizes the log-likelihood function $\mathcal{L} \left(\mathbf{\Gamma} | \widehat{\mathbf{\Gamma}}^{(j-1)} \right) = \mathbb{E}_{\mathbf{h}_b | \mathbf{y}; \widehat{\mathbf{\Gamma}}^{(j-1)}} \{ \log f(\mathbf{y}, \mathbf{h}_b; \mathbf{\Gamma}) \}$, is given by*

$$\widehat{\gamma}_i^{(j)} = \mathbf{R}_b^{(j)}(i, i) + \left| \boldsymbol{\mu}_b^{(j)}(i) \right|^2, \quad (34)$$

where $\boldsymbol{\mu}_b^{(j)} = \mathbf{R}_b^{(j)} \widetilde{\mathbf{\Phi}}^H \mathbf{R}_v^{-1} \mathbf{y} \in \mathbb{C}^{G_R G_T \times 1}$ and $\mathbf{R}_b^{(j)} = \left[\widetilde{\mathbf{\Phi}}^H \mathbf{R}_v^{-1} \widetilde{\mathbf{\Phi}} + \left(\widehat{\mathbf{\Gamma}}^{(j-1)} \right)^{-1} \right]^{-1} \in \mathbb{C}^{G_R G_T \times G_R G_T}$.

Proof. Given in Appendix B. □

The BL algorithm of THz MIMO CSI estimation is summarized in Algorithm 2. The EM procedure is repeated until the estimates of the hyperparameters converge, i.e. the quantity $\left\| \widehat{\mathbf{\Gamma}}^{(j)} - \widehat{\mathbf{\Gamma}}^{(j-1)} \right\|_F^2$ becomes smaller than a suitably chosen threshold ϵ or the number of iterations reaches a maximum limit K_{\max} . The BL-based estimate $\widehat{\mathbf{h}}_{b, \text{BL}}$, upon convergence of the EM procedure, is given by $\widehat{\mathbf{h}}_{b, \text{BL}} = \boldsymbol{\mu}_b^{(j)}$.

A. Multiple Measurement Vector (MMV)-BL (MBL)

Let us now consider a scenario with multiple pilot outputs, denoted by $\mathbf{y}_m, 1 \leq m \leq M$, which are obtained by transmitting an identical pilot matrix \mathbf{X}_p . The output \mathbf{y}_m received from the m th pilot-block transmission can be formulated as $\mathbf{y}_m = \widetilde{\mathbf{\Phi}} \mathbf{h}_{b, m} + \mathbf{v}_m$, where $\mathbf{h}_{b, m}$ represents the beamspace channel corresponding to the m th pilot-block transmission and \mathbf{v}_m is the corresponding noise. Now defining the concatenated matrices $\bar{\mathbf{Y}} = [\mathbf{y}_1 \cdots, \mathbf{y}_M] \in \mathbb{C}^{M_T M_R \times M}$, $\bar{\mathbf{H}}_b = [\mathbf{h}_{b, 1}, \cdots, \mathbf{h}_{b, M}] \in \mathbb{C}^{G_R G_T \times M}$ and $\bar{\mathbf{V}} = [\mathbf{v}_1, \cdots, \mathbf{v}_M]$, the MMV model can be formulated as

$$\bar{\mathbf{Y}} = \widetilde{\mathbf{\Phi}} \bar{\mathbf{H}}_b + \bar{\mathbf{V}}.$$

Furthermore, considering these M pilot-blocks to be well within the *coherence-time* [49], the non-zero locations of the sparse beamspace domain CSI $\mathbf{h}_{b, m}$ do not change. This results in an interesting *simultaneous-sparse* structure of the resultant CSI matrix $\bar{\mathbf{H}}_b$, since its columns $\mathbf{h}_{b, m}$ share an identical sparsity profile. Subsequently, one can derive an MBL framework for efficiently exploiting this simultaneous-sparse structure of the beamspace domain CSI matrix

Algorithm 2 BL-based sparse channel estimation for THz MIMO systems

Input: Pilot output \mathbf{y} , equivalent sensing matrix $\tilde{\Phi}$, noise covariance \mathbf{R}_v , array response dictionary matrices $\mathbf{A}_R(\Phi_R)$ and $\mathbf{A}_T(\Phi_T)$, stopping parameters ϵ and K_{\max}

Initialization: $\hat{\gamma}_i^{(0)} = 1$, for $1 \leq i \leq G_R G_T \Rightarrow \hat{\Gamma}^{(0)} = \mathbf{I}_{G_R G_T}$, $\hat{\Gamma}^{(-1)} = \mathbf{0}$ and counter $j = 0$

while $\left(\left\| \hat{\Gamma}^{(j)} - \hat{\Gamma}^{(j-1)} \right\|_F > \epsilon \text{ and } j < K_{\max} \right)$ **do**

1) $j \leftarrow j + 1$;

2) **E-step:** Compute the *a posteriori* covariance and mean

$$\mathbf{R}_b^{(j)} = \left[\tilde{\Phi}^H \mathbf{R}_v^{-1} \tilde{\Phi} + \left(\hat{\Gamma}^{(j-1)} \right)^{-1} \right]^{-1} \text{ and } \boldsymbol{\mu}_b^{(j)} = \mathbf{R}_b^{(j)} \tilde{\Phi}^H \mathbf{R}_v^{-1} \mathbf{y};$$

3) **M-step:** Update the hyperparameters

for $i = 1, \dots, G_R G_T$ **do**

$$\hat{\gamma}_i^{(j)} = \mathbf{R}_b^{(j)}(i, i) + \left| \boldsymbol{\mu}_b^{(j)}(i) \right|^2$$

end for

end while

$$\hat{\mathbf{h}}_{b, \text{BL}} = \boldsymbol{\mu}_b^{(j)}$$

Output: $\hat{\mathbf{H}}_{\text{BL}} = \mathbf{A}_R(\Phi_R)_{\text{vec}}^{-1} \left(\hat{\mathbf{h}}_{b, \text{BL}} \right) \mathbf{A}_T^H(\Phi_T)$.

$\bar{\mathbf{H}}_b$, which yields a superior estimates. The update equations of the proposed MBL framework for the j th EM iteration is summarized below [50]:

$$\mathbf{R}_b^{(j)} = \left[\tilde{\Phi}^H \mathbf{R}_v^{-1} \tilde{\Phi} + \left(\hat{\Gamma}^{(j-1)} \right)^{-1} \right]^{-1} \text{ and } \hat{\mathbf{H}}^{(j)} = \mathbf{R}_b^{(j)} \tilde{\Phi}^H \mathbf{R}_v^{-1} \bar{\mathbf{Y}},$$

$$\hat{\gamma}_i^{(j)} = \mathbf{R}_b^{(j)}(i, i) + \frac{1}{M} \sum_{m=1}^M \left| \hat{\mathbf{H}}^{(j)}(i, m) \right|^2.$$

Finally, to benchmark the performance, the BCRLB of the CSI estimation model of (29) is derived in the next subsection.

B. BCRLB for THz MIMO Channel Estimation

The Bayesian Fisher information matrix (FIM) $\mathbf{J}_B \in \mathbb{C}^{G_R G_T \times G_R G_T}$ can be evaluated as the sum of FIMs associated with the pilot output \mathbf{y} and the beamspace CSI \mathbf{h}_b , denoted by \mathbf{J}_D and \mathbf{J}_P , respectively. Hence, one can express the Bayesian FIM \mathbf{J}_B as [51]: $\mathbf{J}_B = \mathbf{J}_D + \mathbf{J}_P$, where the matrices \mathbf{J}_D and \mathbf{J}_P are determined as follows. Let the log-likelihoods corresponding to the

THz MIMO beamspace channel \mathbf{h}_b and the pilot output vector \mathbf{y} be represented by $\mathcal{L}(\mathbf{h}_b; \Gamma)$ and $\mathcal{L}(\mathbf{y}|\mathbf{h}_b)$, respectively. These log-likelihoods simplify to

$$\mathcal{L}(\mathbf{y}|\mathbf{h}_b) = \log [f(\mathbf{y}|\mathbf{h}_b)] = c_2 - \left(\mathbf{y} - \tilde{\Phi}\mathbf{h}_b\right)^H \mathbf{R}_v^{-1} \left(\mathbf{y} - \tilde{\Phi}\mathbf{h}_b\right) \quad (35)$$

$$= c_2 - \mathbf{y}^H \mathbf{R}_v^{-1} \mathbf{y} + \mathbf{h}_b^H \tilde{\Phi}^H \mathbf{R}_v^{-1} \mathbf{y} + \mathbf{y}^H \mathbf{R}_v^{-1} \tilde{\Phi} \mathbf{h}_b - \mathbf{h}_b^H \tilde{\Phi}^H \mathbf{R}_v^{-1} \tilde{\Phi} \mathbf{h}_b, \quad (36)$$

$$\mathcal{L}(\mathbf{h}_b; \Gamma) = \log [f(\mathbf{h}_b; \Gamma)] = c_3 - \mathbf{h}_b^H \Gamma^{-1} \mathbf{h}_b, \quad (37)$$

where the terms $c_2 = -M_T M_R \log(\pi) - \log[\det(\mathbf{R}_v)]$ and $c_3 = -G_R G_T \log(\pi) - \log[\det(\Gamma)]$ are constants that do not depend on the beamspace channel \mathbf{h}_b . The FIMs \mathbf{J}_D and \mathbf{J}_P expressed in terms of these log-likelihoods are defined as [51]

$$\mathbf{J}_D = -\mathbb{E}_{\mathbf{y}, \mathbf{h}_b} \left\{ \frac{\partial^2 \mathcal{L}(\mathbf{y}|\mathbf{h}_b)}{\partial \mathbf{h}_b \partial \mathbf{h}_b^H} \right\}, \quad \mathbf{J}_P = -\mathbb{E}_{\mathbf{h}_b} \left\{ \frac{\partial^2 \mathcal{L}(\mathbf{h}_b; \Gamma)}{\partial \mathbf{h}_b \partial \mathbf{h}_b^H} \right\}. \quad (38)$$

The quantity \mathbf{J}_D simplifies to $\mathbf{J}_D = \tilde{\Phi}^H \mathbf{R}_v^{-1} \tilde{\Phi}$, since the (i, j) th element of the Hessian matrix $\frac{\partial^2 \mathcal{L}(\mathbf{y}|\mathbf{h}_b)}{\partial \mathbf{h}_b \partial \mathbf{h}_b^H}$ evaluated as $\frac{\partial^2 \mathcal{L}(\mathbf{y}|\mathbf{h}_b)}{\partial \mathbf{h}_{b,i} \partial \mathbf{h}_{b,j}}$ becomes zero for the initial four terms of (36). As for the last term, the Hessian matrix evaluates to $\tilde{\Phi}^H \mathbf{R}_v^{-1} \tilde{\Phi}$. Similarly, the FIM \mathbf{J}_P evaluates to $\mathbf{J}_P = \Gamma^{-1}$. Thus, the Bayesian FIM \mathbf{J}_B evaluates to $\mathbf{J}_B = \tilde{\Phi}^H \mathbf{R}_v^{-1} \tilde{\Phi} + \Gamma^{-1}$. Finally, the MSE of the estimate $\hat{\mathbf{h}}_b$ can be bounded as

$$\text{MSE}(\hat{\mathbf{h}}_b) = \mathbb{E} \left\{ \left\| \hat{\mathbf{h}}_b - \mathbf{h}_b \right\|^2 \right\} \geq \text{Tr} \{ \mathbf{J}_B^{-1} \} = \text{Tr} \left\{ \left(\tilde{\Phi}^H \mathbf{R}_v^{-1} \tilde{\Phi} + \Gamma^{-1} \right)^{-1} \right\}. \quad (39)$$

Furthermore, upon exploiting the relationship between the CSI vector \mathbf{h} and its beamspace representation \mathbf{h}_b given in (28), one can express the BCRLB for the estimated CSI $\hat{\mathbf{H}}$ as $\text{MSE}(\hat{\mathbf{H}}) \geq \text{Tr} \{ \Psi \mathbf{J}_B^{-1} \Psi^H \}$. The next part of this paper presents the hybrid TPC and RC design using the CSI estimates obtained from the OMP and BL techniques described above.

V. HYBRID TRANSCEIVER DESIGN FOR THZ MIMO SYSTEMS

This treatise develops a novel joint hybrid transceiver design, which directly employs the beamspace channel estimates obtained via the proposed BL-based estimation techniques. Note that the existing mmWave and THz contributions, such as [13], [15], [40], assume the availability of the full CSI for designing the RF precoder $\bar{\mathbf{F}}_{\text{RF}}$ and combiner $\bar{\mathbf{W}}_{\text{RF}}$, which is challenging to obtain due to the large number of antennas and propagation losses. Furthermore, these works either consider the true array response vectors to be perfectly known or employ a codebook for designing the RF precoder/ combiner. To the best of our knowledge, none of the existing papers have directly employed the estimate $\hat{\mathbf{h}}_b$ of the underlying beamspace channel for designing the

hybrid precoder, which is naturally the most suitable approach, given the availability of the beamspace domain channel estimates. The proposed THz hybrid transceiver design addresses this open problem.

A. Hybrid TPC Design

The baseband symbol vector $\bar{\mathbf{x}}$ of (1) comprised of i.i.d. symbols has a covariance matrix given by $\mathbf{R}_{\bar{\mathbf{x}}} = \mathbb{E}\{\bar{\mathbf{x}}\bar{\mathbf{x}}^H\} = \frac{1}{N_s}\mathbf{I}_{N_s}$. The transmit signal vector $\tilde{\mathbf{x}} \in \mathbb{C}^{N_T \times 1}$ is formulated as $\tilde{\mathbf{x}} = \bar{\mathbf{F}}_{\text{RF}}\bar{\mathbf{F}}_{\text{BB}}\bar{\mathbf{x}}$, while the power constraint on the hybrid TPC is given by $\|\bar{\mathbf{F}}_{\text{RF}}\bar{\mathbf{F}}_{\text{BB}}\|_F^2 \leq P_T N_s$, which is equivalent to restricting the total transmit power at the output of the TPC to P_T , yielding $\mathbb{E}\{\tilde{\mathbf{x}}\tilde{\mathbf{x}}^H\} = P_T$. To design the optimal TPCs $\bar{\mathbf{F}}_{\text{BB}}^{\text{opt}} \in \mathbb{C}^{N_{\text{RF}} \times N_s}$ and $\bar{\mathbf{F}}_{\text{RF}}^{\text{opt}} \in \mathbb{C}^{N_T \times N_{\text{RF}}}$, one can maximize the mutual information $\mathcal{I}(\bar{\mathbf{F}}_{\text{BB}}, \bar{\mathbf{F}}_{\text{RF}}) = \log_2 \left| \mathbf{I}_{N_R} + \mathbf{H}\bar{\mathbf{F}}_{\text{RF}}\bar{\mathbf{F}}_{\text{BB}}\bar{\mathbf{F}}_{\text{BB}}^H\bar{\mathbf{F}}_{\text{RF}}^H\mathbf{H}^H \right|$, subject to the power constraint. Thus, the optimization problem of the hybrid TPC can be formulated as

$$\begin{aligned} \{\bar{\mathbf{F}}_{\text{BB}}^{\text{opt}}, \bar{\mathbf{F}}_{\text{RF}}^{\text{opt}}\} &= \arg \max_{(\bar{\mathbf{F}}_{\text{BB}}, \bar{\mathbf{F}}_{\text{RF}})} \log_2 \left| \mathbf{I}_{N_R} + \mathbf{H}\bar{\mathbf{F}}_{\text{RF}}\bar{\mathbf{F}}_{\text{BB}}\bar{\mathbf{F}}_{\text{BB}}^H\bar{\mathbf{F}}_{\text{RF}}^H\mathbf{H}^H \right|, \\ \text{s.t.} \quad &\|\bar{\mathbf{F}}_{\text{RF}}\bar{\mathbf{F}}_{\text{BB}}\|_F^2 \leq P_T N_s, |\bar{\mathbf{F}}_{\text{RF}}(i, j)| = \frac{1}{\sqrt{N_T}}, 1 \leq i \leq N_T, 1 \leq j \leq N_{\text{RF}}. \end{aligned} \quad (40)$$

Note that the above optimization problem is non-convex owing to the non-linear constraints on the elements of $\bar{\mathbf{F}}_{\text{RF}}$, which renders it intractable. To circumvent this problem, one can initially design the optimal fully-digital TPC $\bar{\mathbf{F}} \in \mathbb{C}^{N_T \times N_s}$ via the substitution $\bar{\mathbf{F}}_{\text{RF}}\bar{\mathbf{F}}_{\text{BB}} = \bar{\mathbf{F}}$ in the above optimization problem and ignoring the constant magnitude constraints. Upon obtaining the fully-digital TPC $\bar{\mathbf{F}}^{\text{opt}}$, one can then decompose it into its RF and baseband constituents represented by the matrices $\bar{\mathbf{F}}_{\text{RF}}^{\text{opt}}$ and $\bar{\mathbf{F}}_{\text{BB}}^{\text{opt}}$, respectively. The well-known water-filling solution for design of the fully-digital TPC is as follows.

Let $\mathbf{H} = \mathbf{U}\mathbf{\Sigma}\mathbf{V}^H$ represent the singular value decomposition (SVD) of the THz MIMO channel. The optimal fully-digital TPC $\bar{\mathbf{F}}^{\text{opt}}$ is expressed as

$$\bar{\mathbf{F}}^{\text{opt}} = \mathbf{V}_1 \mathbf{P}^{1/2}, \quad (41)$$

where $\mathbf{V}_1 = \mathbf{V}(:, 1 : N_s) \in \mathbb{C}^{N_T \times N_s}$ and the matrix $\mathbf{P} \in \mathbb{R}_+^{N_s \times N_s}$ represents a diagonal power allocation matrix, whose i th diagonal element $p_i, 1 \leq i \leq N_s$, can be derived as $p_i = \max \left\{ 0, \left(\lambda - \frac{\sigma_v^2}{(\Sigma(i, i))^2} \right) \right\}$. The quantity λ denotes the Lagrangian multiplier [52], which satisfies the power constraint $\sum_{i=1}^{N_s} p_i \leq P_T N_s$. Subsequently, the optimal hybrid TPCs $\bar{\mathbf{F}}_{\text{BB}}^{\text{opt}}$ and

Algorithm 3 Hybrid transceiver design from the estimated beamspace THz MIMO channel $\widehat{\mathbf{h}}_b$

Input: Estimated beamspace channel $\widehat{\mathbf{h}}_b$, optimal fully-digital TPC $\bar{\mathbf{F}}^{\text{opt}}$ and MMSE RC $\bar{\mathbf{W}}_M$, output covariance matrix \mathbf{R}_{yy} , number of RF chains N_{RF} , array response dictionary matrices $\mathbf{A}_R(\Phi_R)$ and $\mathbf{A}_T(\Phi_T)$

Initialization: $\bar{\mathbf{F}}_{\text{RF}} = [\]$, $\bar{\mathbf{W}}_{\text{RF}} = [\]$, $\mathbf{h}_{b,\text{abs}} = |\widehat{\mathbf{h}}_b|$, construct an ordered set \mathcal{S} from the indices of elements of the vector $\mathbf{h}_{b,\text{abs}}$, so that $\mathbf{h}_{b,\text{abs}}[\mathcal{S}(1)] \geq \mathbf{h}_{b,\text{abs}}[\mathcal{S}(2)] \geq \mathbf{h}_{b,\text{abs}}[\mathcal{S}(3)] \geq \dots \geq \mathbf{h}_{b,\text{abs}}[\mathcal{S}(G_R G_T)]$

for $i = 1, 2, \dots, N_{\text{RF}}$

1) $j = \text{floor}[(\mathcal{S}(i) - 1) / G_R] + 1$; $k = \text{rem}[(\mathcal{S}(i) - 1), G_R] + 1$;

2) $\bar{\mathbf{F}}_{\text{RF}} = [\bar{\mathbf{F}}_{\text{RF}} \ \mathbf{a}_t(\phi_j)]$; $\bar{\mathbf{W}}_{\text{RF}} = [\bar{\mathbf{W}}_{\text{RF}} \ \mathbf{a}_r(\phi_k)]$;

end for

$\bar{\mathbf{F}}_{\text{BB}} = (\bar{\mathbf{F}}_{\text{RF}})^\dagger \bar{\mathbf{F}}^{\text{opt}}$; $\bar{\mathbf{W}}_{\text{BB}} = (\bar{\mathbf{W}}_{\text{RF}}^H \mathbf{R}_{yy} \bar{\mathbf{W}}_{\text{RF}})^{-1} \bar{\mathbf{W}}_{\text{RF}}^H \mathbf{R}_{yy} \bar{\mathbf{W}}_M$;

Output: $\bar{\mathbf{F}}_{\text{BB}}$, $\bar{\mathbf{F}}_{\text{RF}}$, $\bar{\mathbf{W}}_{\text{BB}}$, $\bar{\mathbf{W}}_{\text{RF}}$

$\bar{\mathbf{F}}_{\text{RF}}^{\text{opt}}$ can be obtained from the optimal fully-digital TPC $\bar{\mathbf{F}}^{\text{opt}}$ as the solution of the approximate problem [24]

$$\begin{aligned} \{\bar{\mathbf{F}}_{\text{BB}}^{\text{opt}}, \bar{\mathbf{F}}_{\text{RF}}^{\text{opt}}\} &= \arg \min_{(\bar{\mathbf{F}}_{\text{BB}}, \bar{\mathbf{F}}_{\text{RF}})} \|\bar{\mathbf{F}}^{\text{opt}} - \bar{\mathbf{F}}_{\text{RF}} \bar{\mathbf{F}}_{\text{BB}}\|_F^2, \\ \text{s.t.} \quad &\|\bar{\mathbf{F}}_{\text{RF}} \bar{\mathbf{F}}_{\text{BB}}\|_F^2 \leq P_T N_S, \quad |\bar{\mathbf{F}}_{\text{RF}}(i, j)| = \frac{1}{\sqrt{N_T}}. \end{aligned} \quad (42)$$

Although the above optimization problem is non-convex, the following interesting observation substantially simplifies hybrid TPC design. Note that the THz MIMO channel of (2) can be compactly represented as $\mathbf{H} = \bar{\mathbf{A}}_R \mathbf{D} \bar{\mathbf{A}}_T^H$, where $\bar{\mathbf{A}}_R \in \mathbb{C}^{N_R \times (N_{\text{LoS}} + 1) N_{\text{ray}}}$ and $\bar{\mathbf{A}}_T \in \mathbb{C}^{N_T \times (N_{\text{LoS}} + 1) N_{\text{ray}}}$ are the matrices that comprise $(N_{\text{LoS}} + 1) N_{\text{ray}}$ array response vectors corresponding to the AoAs and AoDs of all the multipath components, respectively, whereas the diagonal matrix $\mathbf{D} \in \mathbb{C}^{(N_{\text{LoS}} + 1) N_{\text{ray}} \times (N_{\text{LoS}} + 1) N_{\text{ray}}}$ contains their complex path-gains. Thus, the row- and column-spaces of the channel matrix \mathbf{H} obey

$$\mathcal{R}(\mathbf{H}^*) = \mathcal{C}(\bar{\mathbf{A}}_T), \quad \mathcal{C}(\mathbf{H}) = \mathcal{C}(\bar{\mathbf{A}}_R), \quad (43)$$

where $\mathcal{R}(\cdot)$ and $\mathcal{C}(\cdot)$ represent the row and column spaces, respectively, of a matrix. At this juncture, using the SVD of \mathbf{H} together with (41), one can conclude that

$$\mathcal{C}(\mathbf{F}^{\text{opt}}) \subseteq \mathcal{C}(\mathbf{V}_1) \subseteq \mathcal{C}(\mathbf{V}(:, 1 : \rho)) = \mathcal{R}(\mathbf{H}^*), \quad (44)$$

where we have $\rho = \text{rank}(\mathbf{H})$ and $\rho \geq N_S$. Hence, from (43) and (44), one can deduce that

$$\mathcal{C}(\bar{\mathbf{F}}^{\text{opt}}) \subseteq \mathcal{C}(\bar{\mathbf{A}}_T). \quad (45)$$

This implies that a suitable linear combination of the columns of $\bar{\mathbf{A}}_T$ can determine any column of the matrix $\bar{\mathbf{F}}^{\text{opt}}$. Furthermore, since it is evident that the array response vectors \mathbf{a}_t also satisfy the non-convex constraints of (42), courtesy (6), the columns of the matrix $\bar{\mathbf{A}}_T$ are a suitable candidate for the RF TPC $\bar{\mathbf{F}}_{\text{RF}}$. However, a pair of key challenges remain. Firstly, the array response matrix $\bar{\mathbf{A}}_T$ is unknown. To compound this problem, one can only choose N_{RF} columns of $\bar{\mathbf{A}}_T$ for the design of the RF TPC, owing to the fact that there are only N_{RF} RF chains. Both the above-mentioned issues can be efficiently addressed by employing the estimate $\hat{\mathbf{h}}_b$ of the beamspace channel as follows.

Note that the dominant coefficients of the beamspace channel matrix \mathbf{H}_b (c.f. (27)) represent the active (AoA, AoD)-pairs. Therefore, to design the RF TPC $\bar{\mathbf{F}}_{\text{RF}}$, one can directly employ the estimate $\hat{\mathbf{H}}_b$ of the beamspace channel matrix derived from the estimation techniques proposed in Section-III-B and IV. The salient steps in the proposed hybrid transceiver design procedure are detailed in Algorithm 3. We commence by arranging the elements of the quantity $|\hat{\mathbf{h}}_b|$ in descending order and determine the N_{RF} entries that have the highest magnitude. The corresponding locations in the beamspace matrix representation yield the active (AoA, AoD)-pairs. More precisely, the column indices, represented by j in Step-1 of Algorithm 3, provide the active AoDs in the transmit angular grid Φ_T , whereas the row indices, denoted by k , yield the active AoAs. The RF TPC $\bar{\mathbf{F}}_{\text{RF}}$ can be subsequently constructed from the N_{RF} -dominant columns of the transmit array response dictionary matrix $\mathbf{A}_T(\Phi_T)$ (c.f. (25)). Finally, the baseband TPC $\bar{\mathbf{F}}_{\text{BB}}$ can be obtained from the LS estimate as $\bar{\mathbf{F}}_{\text{BB}} = (\bar{\mathbf{F}}_{\text{RF}})^\dagger \bar{\mathbf{F}}^{\text{opt}}$. The procedure of the hybrid RC design in THz MIMO systems is described next.

B. Hybrid MMSE RC Design

This subsection describes the design of the hybrid MMSE RC components $\bar{\mathbf{W}}_{\text{BB}} \in \mathbb{C}^{N_{\text{RF}} \times N_S}$ and $\bar{\mathbf{W}}_{\text{RF}} \in \mathbb{C}^{N_R \times N_{\text{RF}}}$ relying on the estimated beamspace channel matrix $\hat{\mathbf{H}}_b$. Toward this, for a given hybrid TPC $\bar{\mathbf{F}}_{\text{BB}}$ and $\bar{\mathbf{F}}_{\text{RF}}$, one can minimize the MSE of approximation between the transmit baseband symbol vector $\bar{\mathbf{x}} \in \mathbb{C}^{N_S \times 1}$ and the output $\bar{\mathbf{y}}$, which obey (1), subject to the

constant-magnitude constraints on the elements of the RF RC $\bar{\mathbf{W}}_{\text{RF}}$. Let $\mathbf{y} \in \mathbb{C}^{N_R \times 1}$ denote the signal impinging at the RAs, which is given by

$$\mathbf{y} = \mathbf{H}\bar{\mathbf{F}}_{\text{RF}}\bar{\mathbf{F}}_{\text{BB}}\bar{\mathbf{x}} + \bar{\mathbf{v}}.$$

Thus, the RC design optimization problem can be formulated as

$$\begin{aligned} \{\bar{\mathbf{W}}_{\text{RF}}^{\text{opt}}, \bar{\mathbf{W}}_{\text{BB}}^{\text{opt}}\} &= \arg \min_{(\bar{\mathbf{W}}_{\text{RF}}, \bar{\mathbf{W}}_{\text{BB}})} \mathbb{E} \left\{ \|\bar{\mathbf{x}} - \bar{\mathbf{W}}_{\text{BB}}^H \bar{\mathbf{W}}_{\text{RF}}^H \mathbf{y}\|_2^2 \right\}, \\ \text{s.t.} \quad & |\bar{\mathbf{W}}_{\text{RF}}(i, j)| = \frac{1}{\sqrt{N_R}}. \end{aligned} \quad (46)$$

As detailed in Appendix C, the above optimization problem can be reformulated as

$$\begin{aligned} \{\bar{\mathbf{W}}_{\text{RF}}^{\text{opt}}, \bar{\mathbf{W}}_{\text{BB}}^{\text{opt}}\} &= \arg \min_{(\bar{\mathbf{W}}_{\text{RF}}, \bar{\mathbf{W}}_{\text{BB}})} \|\mathbf{R}_{yy}^{1/2} (\bar{\mathbf{W}}_{\text{M}} - \bar{\mathbf{W}}_{\text{RF}} \bar{\mathbf{W}}_{\text{BB}})\|_F^2 \\ \text{s.t.} \quad & |\bar{\mathbf{W}}_{\text{RF}}(i, j)| = \frac{1}{\sqrt{N_R}}, \end{aligned} \quad (47)$$

where the matrices $\mathbf{R}_{yy} \in \mathbb{C}^{N_R \times N_R}$ and $\bar{\mathbf{W}}_{\text{M}} \in \mathbb{C}^{N_R \times N_S}$ represent the covariance matrix of the output vector \mathbf{y} and the optimal MMSE RC, respectively. These can be formulated as

$$\mathbf{R}_{yy} = \mathbf{E} \{\mathbf{y}\mathbf{y}^H\} = \frac{1}{N_S} (\mathbf{H}\bar{\mathbf{F}}_{\text{RF}}\bar{\mathbf{F}}_{\text{BB}}\bar{\mathbf{F}}_{\text{BB}}^H\bar{\mathbf{F}}_{\text{RF}}^H\mathbf{H}^H + N_S\sigma_v^2\mathbf{I}_{N_R}), \quad (48)$$

$$\bar{\mathbf{W}}_{\text{M}} = \mathbf{H}\bar{\mathbf{F}}_{\text{RF}}\bar{\mathbf{F}}_{\text{BB}} (\bar{\mathbf{F}}_{\text{BB}}^H\bar{\mathbf{F}}_{\text{RF}}^H\mathbf{H}^H\mathbf{H}\bar{\mathbf{F}}_{\text{RF}}\bar{\mathbf{F}}_{\text{BB}} + N_S\sigma_v^2\mathbf{I}_{N_S})^{-1}. \quad (49)$$

Since we have $\mathcal{C}(\bar{\mathbf{W}}_{\text{M}}) \subseteq \mathcal{C}(\mathbf{H}) = \mathcal{C}(\bar{\mathbf{A}}_R)$, similar to the simplified TPC design, one can design the RF RC $\bar{\mathbf{W}}_{\text{RF}}$ from the array response vectors of the N_{RF} active AoAs obtained from the estimated beamspace channel. Finally, the baseband RC $\bar{\mathbf{W}}_{\text{BB}}$ can be derived using the following weighted-LS solution: $\bar{\mathbf{W}}_{\text{BB}} = (\bar{\mathbf{W}}_{\text{RF}}^H \mathbf{R}_{yy} \bar{\mathbf{W}}_{\text{RF}})^{-1} \bar{\mathbf{W}}_{\text{RF}}^H \mathbf{R}_{yy} \bar{\mathbf{W}}_{\text{M}}$. For convenience, the hybrid RC design is also presented in Algorithm 3. Note that a key advantage of the proposed hybrid MMSE RC design is that the processed signal $\bar{\mathbf{y}} = \bar{\mathbf{W}}_{\text{BB}}^H \bar{\mathbf{W}}_{\text{RF}}^H \mathbf{y}$ directly yields the MMSE estimate of the transmit symbol vector $\bar{\mathbf{x}}$.

Note that the SOMP technique, as described in [15], requires N_{RF} iterations for selecting the N_{RF} dominant array response vectors via a computationally intensive correlation method (Step-4 and 5 of Algorithm-1 in [15]), followed by an intermediate LS solution in each iteration. By contrast, the proposed hybrid precoder design framework is directly able to compute the final baseband precoder using the LS solution, once the RF precoder is derived using the estimated beamspace domain CSI. Thus, the proposed hybrid precoder design has a significantly lower computational cost, while performing very close to the ideal fully-digital benchmark,

as demonstrated in our simulation results of Fig. 3 and Fig. 4. Furthermore, the framework for beamspace domain CSI estimation, followed by our hybrid transceiver design developed requires significantly lower feedback, since the receiver only has to feed back a few indices of the dominant beamspace components together with their quantized gains in order to construct the hybrid precoder of the transmitter.

The objectives of the proposed hybrid transceiver optimization problems in (40) and (46) of this treatise are to design a capacity-optimal hybrid precoder and MMSE-optimal hybrid combiner. We would like to clarify that the proposed solution does not guarantee optimality, since our solution directly employs the estimate $\hat{\mathbf{h}}_b$ of the beamspace domain channel obtained from the proposed BL-based CSI estimators. Hence, its performance heavily relies on the estimated CSI, as demonstrated in our simulation results of Fig. 3 and 4, which will always be the case for any practical solution developed for this problem. However, a solid mathematical foundation established after (42) justifies its low complexity and significantly improved performance that is close to the corresponding optimal fully-digital solution. On the other hand, the existing optimization algorithms conceived for hybrid transceiver design, such as [20], [21], may guarantee certain optimality, but they are typically iterative and computationally complex.

C. Computational Complexity

This subsection derives the computational cost of the proposed THz hybrid MIMO transceiver design, which is directly coupled with the beamspace domain CSI estimation module. The computational complexity order of the BL technique may be shown to be $\mathcal{O}(G_R^3 G_T^3)$, which arises due to the matrix inversion of size- $[G_R G_T \times G_R G_T]$. On the other hand, the worst-case complexity order of the OMP scheme is seen to be $\mathcal{O}(M_T^3 M_R^3)$, which arises due to the intermediate LS estimate required in each iteration. Finally, the computational cost of the hybrid transceiver design presented in Algorithm-3 based on the estimated BL-based CSI is seen to be on the order of $\mathcal{O}(N_T^3 + N_{\text{RF}}^3 + N_S^3)$. Here, the $\mathcal{O}(N_T^3)$ term arises due to the SVD of the THz MIMO channel \mathbf{H} , $\mathcal{O}(N_{\text{RF}}^3)$ is due to the LS solution of the baseband precoder $\bar{\mathbf{F}}_{\text{BB}}$ and combiner $\bar{\mathbf{W}}_{\text{BB}}$, whereas $\mathcal{O}(N_S^3)$ is due to the calculation of the fully-digital MMSE solution in (49). Thus, it can be readily observed that the overall computational cost of obtaining the OMP-based estimated CSI followed by the hybrid transceiver design is lower than that of employing the BL-based estimated CSI. However, as discussed later in our simulation results, the performance of the proposed hybrid transceiver design using OMP-based CSI is poor in

comparison to that obtained via the BL-based CSI for an identical pilot overhead. Hence, there is a trade-off between the computational cost and the performance improvement attained.

VI. SIMULATION RESULTS

The performance of the proposed CSI estimation techniques conceived for our hybrid THz MIMO transceiver design is illustrated by our simulation results. For this study, the magnitudes of the LoS and NLoS complex path-gains $\alpha(f, d)$ have been generated using (7) and (9), respectively, whereas the associated phase shifts ψ are generated as i.i.d. samples of a random variable uniformly distributed over the interval $(-\pi, \pi]$. The molecular absorption coefficient $k_{\text{abs}}(f)$ has been computed using the procedure described in Section-II-C relying on the HITRAN database [10]. The operating carrier frequency f and the transmission distance d are set to 0.3 THz and 10 m, respectively, unless stated otherwise. Furthermore, an office scenario is considered with the system pressure p and temperature T set to 1 atm and 296 K, respectively, which has the following molecular composition: water vapour (1%), oxygen (20.9%) and nitrogen (78.1%). The THz MIMO channel is generated using a single LoS and $N_{\text{NLoS}} = 4$ NLoS components, in which 3 NLoS components have first-order reflections, whereas the 4th NLoS component is assumed to have a second-order reflection from the respective scatterer. Furthermore, each multipath component is composed of $N_{\text{ray}} \in \{1, 3\}$ diffused rays, whose AoAs/ AoDs follow i.i.d. Gaussian distributions with an angular spread of standard deviation of $1/10$ radian around the mean angle of the particular multipath component [53]. The standard deviation of the roughness of various reflecting media is set as $\sigma \in \{0.05, 0.13, 0.15\}$ mm [44]. The TA and RA gains, G_t^a and G_r^a , respectively, are set to $G_t^a = G_r^a = 25$ dB. Given the various channel parameters mentioned above, the THz MIMO channel has been generated using (2)-(4).

For simulation, this work considers two THz MIMO systems, namely System-I and System-II, having the simulation parameters described below. For System-I, the number of TAs/ RAs is set to $N_T = N_R = 32$ with $N_{\text{RF}} = 8$ RF chains at both the ends. The number of training vectors, M_T and M_R , is set to $M_T = M_R = 24$, which can be seen to be lower than N_T and N_R . The angular grid sizes, G_T and G_R , for this system are set as $G_T = G_R = 36$, which is higher than $\max(N_T, N_R)$. By contrast, the simulation parameters of System-II are as follows: $N_T = N_R = 16$, $N_{\text{RF}} = 4$, $M_T = M_R = 12$ and $G_T = G_R = 20$. Note that, in contrast to the conventional channel estimation models, which are typically over-determined, the setting for System-I results in a $[576 \times 1296]$ -size equivalent sensing matrix $\tilde{\Phi}$, thus leading to an under-

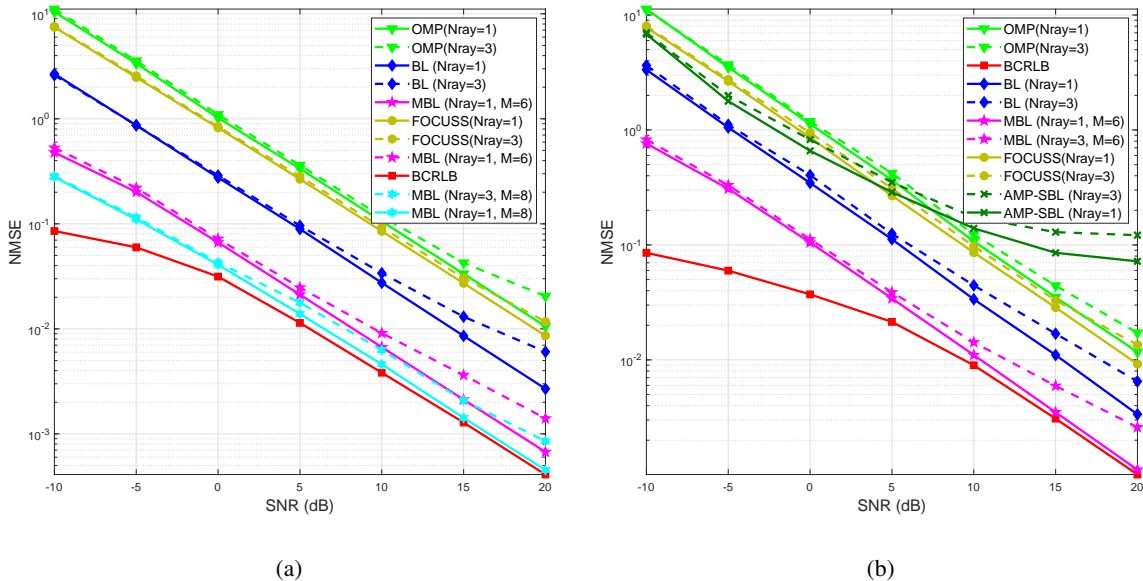


Fig. 2: NMSE versus SNR comparison for a THz MIMO (a) System-I; (b) System-II.

determined system, as described by Eq. (29). However, as shown in the simulation results, the proposed sparse estimation techniques developed in our paper are able to estimate the THz MIMO CSI with the desired accuracy even in such a challenging scenario. Furthermore, the antenna spacings, d_t and d_r , for both the Systems have been set to $d_t = d_r = \frac{\lambda}{2}$. The SNR is defined as $\text{SNR} = 10 \log_{10} \left(\frac{1}{\sigma_v^2} \right)$ dB. For the OMP technique, the stopping parameter ϵ_t is set to $\epsilon_t = \sigma_v^2$, whereas for the BL technique, we set $\epsilon = 10^{-6}$ and $K_{\max} = 50$.

A. THz Hybrid MIMO Channel Estimation

Fig. 2(a) and Fig. 2(b) illustrate the sparse channel estimation performance versus SNR for the THz MIMO System-I and System-II, respectively, in terms of the normalized MSE (NMSE), which is defined as $\text{NMSE} = \frac{\|\hat{\mathbf{H}} - \mathbf{H}\|_F^2}{\|\mathbf{H}\|_F^2}$. The performance of the proposed OMP and BL-based algorithms is also compared to that of the popular sparse signal recovery technique FOCal Underdetermined System Solver (FOCUSS) [54], typically used in the field of image reconstruction. The performance of all the competing techniques is also benchmarked against the BCRLB, as derived in Section-IV-B. From both the figures, one can conclude that the proposed BL-based sparse channel estimation technique outperforms the OMP and FOCUSS, which is attributed to its robustness toward the tolerance parameter ϵ and K_{\max} , and toward the dictionary

matrix $\tilde{\Phi}$. On the other hand, the sensitivity of the OMP technique to the stopping threshold ϵ_t and to the dictionary matrix lead to structural and convergence errors, as described in [47], thus degrading the eventual sparse recovery of the beamspace channel. Furthermore, the OMP technique suffers due to its greedy nature and error propagation, since the error encountered in the selection of the indices cannot be rectified in the subsequent iterations, thus negatively impacting its performance. On the other hand, the performance of FOCUSS is poor due to its convergence deficiencies and sensitivity to the regularization parameter [47]. The proposed techniques are also compared to low-complexity approximate message passing (MP)-based sparse Bayesian learning (AMP-SBL) [55], which is the Bayesian extension of the MP algorithms developed in [56], [57]. The performance of the AMP-SBL algorithm is poor in comparison to the proposed BL algorithm, since it only tracks the *a posteriori* mean and variance of each element of the sparse vector, leading to its sub-optimal performance, especially at high SNR. One can also note from Fig. 2(a) that the proposed MMV-BL (MBL) technique approaches the BCRLB upon increasing the number of measurements M . This is significant, since the BCRLB is derived for an ideal scenario, where the AoAs/ AoDs are perfectly known, whereas the BL framework does not rely on this idealized simplifying assumption. Another interesting observation is as follows. When the THz MIMO channel has $N_{ray} = 3$ diffused rays, the performance of all the competing schemes degrades. The reason behind this degradation is that the diffused rays lead to broadening the beamwidth of the AoAs/ AoDs, which essentially increases the support of the beamspace channel, eventually degrading the performance of sparse signal recovery. However, one can also verify that this degradation is minimal for the proposed BL scheme, which outperforms the others in this scenario as well. Furthermore, one can also note that the proposed sparse estimation frameworks are capable of accurately estimating the $N_R \times N_T$ THz MIMO channel using M_T and M_R beam-patterns, where $M_T M_R \ll N_T N_R$. It is plausible that this is not possible using the conventional LS and MMSE schemes, as described in Section-III. Thus, its superior CSI estimation performance coupled with its lower pilot overhead make the proposed BL-based sparse estimation framework ideally suited for THz MIMO systems.

B. THz MIMO Hybrid Transceiver Design

This subsection evaluates both the ASE in bits/sec/Hz and the BER to illustrate the performance of the proposed hybrid transceiver design. The ASE is computed using the well-known Shannon capacity formula as $C = \log_2 \left| \mathbf{I}_{N_S} + \frac{1}{N_S} \mathbf{R}_n^{-1} \mathbf{H}_{\text{eq}} \mathbf{H}_{\text{eq}}^H \right|$, where the matrices

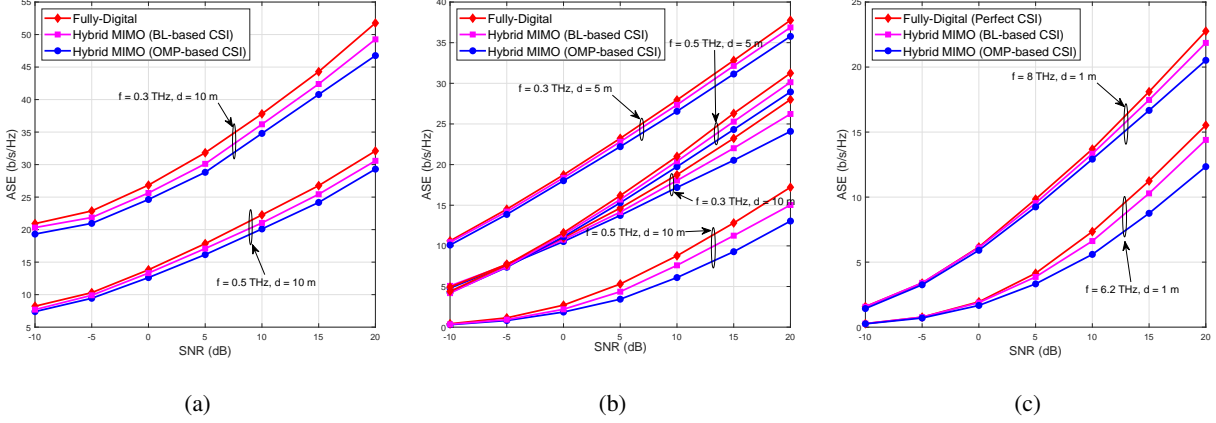


Fig. 3: ASE versus SNR comparison for a THz MIMO, (a) System-I; (b) System-II, with different frequencies and distances; (c) Effect of molecular absorption losses on ASE

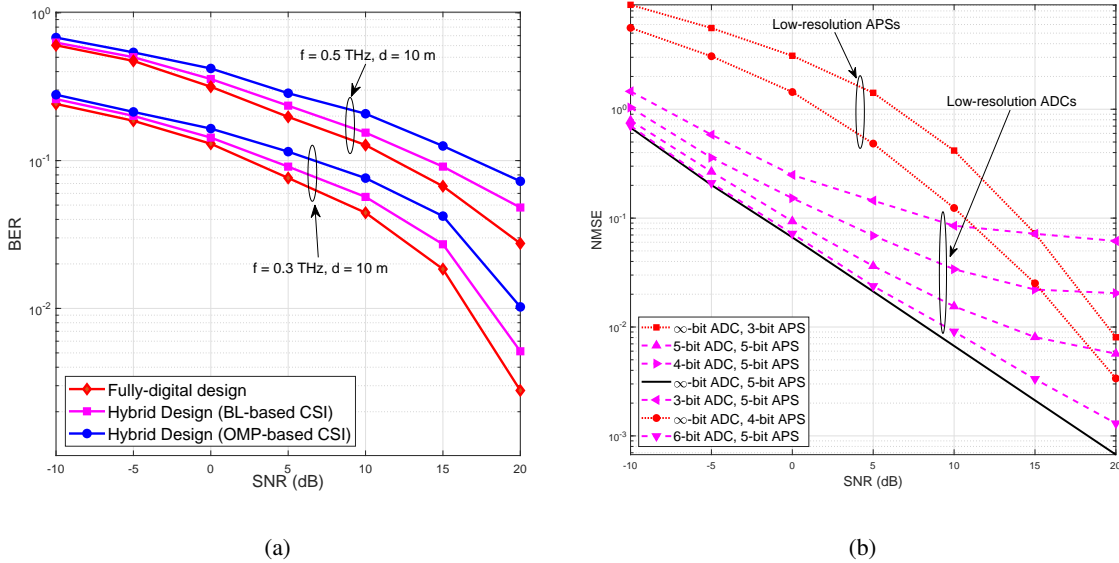


Fig. 4: (a) BER versus SNR comparison, for THz MIMO System-II; (b) NMSE versus SNR comparison for a THz MIMO System-I considering low-resolution ADCs and APSs.

\mathbf{R}_n and \mathbf{H}_{eq} denote the covariance of the combined noise and equivalent baseband channel, respectively, given by $\mathbf{R}_n = \sigma_v^2 \bar{\mathbf{W}}_{\text{BB}}^H \bar{\mathbf{W}}_{\text{RF}}^H \bar{\mathbf{W}}_{\text{RF}} \bar{\mathbf{W}}_{\text{BB}}$, $\mathbf{H}_{\text{eq}} = \bar{\mathbf{W}}_{\text{BB}}^H \bar{\mathbf{W}}_{\text{RF}}^H \bar{\mathbf{H}} \bar{\mathbf{F}}_{\text{RF}} \bar{\mathbf{F}}_{\text{BB}}$. The quantities $\bar{\mathbf{W}}_{\text{RF}}$, $\bar{\mathbf{W}}_{\text{BB}}$, $\bar{\mathbf{F}}_{\text{RF}}$ and $\bar{\mathbf{F}}_{\text{BB}}$ have been evaluated using the proposed hybrid transceiver design described in Algorithm-3, which in turn requires the estimated beamspace domain CSI obtained from the OMP (Algorithm-1) or BL (Algorithm-2) schemes. The ASE of a fully-digital THz MIMO system having perfect CSI is also plotted therein to benchmark the performance and to

demonstrate the gap between the proposed hybrid and ideal baseband transceiver architectures.

Fig. 3(a) plots the ASE versus SNR for System-I. Observe that the proposed hybrid transceiver design using the estimated beamspace domain CSI yields an ASE that is reasonably close to that of the fully-digital system having perfect CSI. This demonstrates the efficacy of the proposed hybrid transceiver design as well as that of the OMP and BL-based sparse CSI estimation techniques. The improved CSI estimation accuracy of the BL technique also leads to higher ASE in comparison to the same achieved using OMP-based CSI. Furthermore, the ASE is also plotted for two different frequencies, viz., $f \in \{0.3, 0.5\}$ THz. Observe from the figure that due to the high free-space losses characterized by (8), the ASE of the THz MIMO system at the higher operating frequency $f = 0.5$ THz is lower than that at $f = 0.3$ THz, for a given transmission distance of $d = 10$ m. A similar observation can be made in Fig. 3(b) for System-II, where the effect of varying the transmission distance is also presented. Once again, due to the high free-space losses, the ASE of the THz MIMO system at the higher transmission distance of $d = 10$ m is lower than at $d = 5$ m. Fig. 3(c) illustrates another interesting result by considering the pair of frequencies $f \in \{6.2, 8.0\}$ THz for the same transmission distance of $d = 1$ m. Note that the ASE of the THz MIMO system for $f = 6.2$ THz is lower than at $f = 8.0$ THz, which is in contrast to the results of Figs. 3(a)-(b). Following the procedure described in Section-II-C and employing the HITRAN database, the molecular absorption coefficients $k_{\text{abs}}(f)$ at $f = 6.2$ THz and 8.0 THz approximately evaluate to $\approx 3.1 \text{ m}^{-1}$ and $\approx 0.3 \text{ m}^{-1}$, respectively. Hence, the poor performance at $f = 6.2$ THz can be attributed to the higher molecular absorption losses at this operating frequency, which is a characteristic feature of the THz MIMO channel. Therefore, in order to precisely characterize the system performance at a specific frequency, one must consider the effect of the molecular absorption coefficient $k_{\text{abs}}(f)$ and the associated losses $L_{\text{abs}}(f, d)$, as described in (8). Finally, Fig. 4(a) plots the BER versus SNR using the proposed hybrid transceiver design for quadrature-phase shift keying (QPSK) modulation. A similar trend is observed, where the proposed design using the BL-based estimated CSI yields a BER sufficiently close to the benchmark. Furthermore, the BER of the THz MIMO system at $f = 0.3$ THz is lower than at $f = 0.5$ THz.

C. Effects of Low-Resolution ADCs and APSs

Fig. 4(b) analyzes the effects of employing low-resolution ADCs on the CSI estimation performance of the proposed BL-based approaches. For this, the quantized pilot output y_q

corresponding to the pilot output \mathbf{y} of (29) is expressed as $\mathbf{y}_q = \mathcal{Q}(\mathbf{y})$, where $\mathcal{Q}(\cdot)$ represents the element-wise quantization operator. Hence, the i th element $y_q(i)$ of the quantized pilot output is given as

$$y_q(i) = \mathcal{Q}(\text{Real}[\mathbf{y}(i)]) + j\mathcal{Q}(\text{Imag}[\mathbf{y}(i)]).$$

Note that for a b_q -bit quantizer, the number of levels $N_q = 2^{b_q}$, which implies that the quantizer output $\mathcal{Q}(y)$ for any scalar $y \in \mathbb{R}$ is given as

$$\mathcal{Q}(y) = \begin{cases} v_1, & y \in [u_0, u_1]; \\ v_2, & y \in (u_1, u_2]; \\ \vdots & \vdots \\ v_{N_q}, & y \in (u_{N_q-1}, u_{N_q}], \end{cases}$$

where $u_0 < u_1 < \dots < u_{N_q}$ denote the quantization thresholds, whereas $\{v_i\}_{i=1}^{N_q}$ represent the quantizer output levels. For simplicity, we consider a uniform mid-point quantizer, which obeys

$$u_i = (-N_q/2 + i)\Delta, \quad i = 0, \dots, N_q,$$

$$v_i = (u_{i-1} + u_i)/2, \quad i = 1, \dots, N_q,$$

where Δ denotes the quantization step-size. Furthermore, the model for the quantized pilot output \mathbf{y}_q can be expressed as

$$\mathbf{y}_q = \tilde{\Phi} \mathbf{h}_b + \mathbf{v} + \mathbf{v}_q,$$

where \mathbf{v}_q denotes the additional quantization noise. The NMSE performance of the proposed sparse channel estimation schemes considering different ADC resolutions is illustrated in Fig. 4(b). One can readily observe that the NMSEs of the proposed techniques for $b_q = 6$ -bit ADC resolution are almost identical to that of the ∞ -bit resolution, i.e. for the analog pilot outputs. Furthermore, the NMSE increases upon decreasing the ADC resolution, which is attributed to the increased quantization noise. However, for the low SNR regime of -10 dB to 10 dB, which is a typical scenario in the THz band, the NMSEs achieved for 4- and 3-bit ADC resolutions are still acceptable. This demonstrates the feasibility of the proposed CSI estimation schemes for practical THz hybrid MIMO systems also, which demand low-resolution ADCs due to their high bandwidth for the sake of reducing their power consumption.

Fig. 4(b) also demonstrates the effects of using low-resolution APSs on the CSI estimation performance. Note that setting the RF TPC and RC using the DFT matrices requires $\log_2(N_T)$ - and $\log_2(N_R)$ -bit APSs, respectively. Thus, 5-bit APSs are sufficient for an efficient sparse CSI

estimation in a THz hybrid MIMO system having $N_T = N_R = 32$ antennas. Furthermore, the proposed CSI estimation model is general, and it can also operate with APSs having further low resolution of 3-bit and 4-bit, as seen in the Fig. 4(b).

VII. CONCLUSIONS

This work developed a practical MIMO channel model considering several key aspects of the THz band, such as the reflection losses and molecular absorption. Then a sparse CSI estimation model was developed for exploiting the underlying angular-sparsity of the THz MIMO channel, followed by the OMP and improved BL-based frameworks for CSI estimation. Furthermore, the BCRLB was also determined for benchmarking the performance of the proposed channel estimation techniques. Finally, optimal hybrid TPC and RC designs were developed, which directly employ the estimated beamspace domain CSI and require only limited CSI feedback. Our simulation setup employed practical THz MIMO channel parameters obtained from the HITRAN-database. The proposed BL framework was seen to yield both an MSE performance close to the BCRLB and an improved ASE. Furthermore, the proposed frameworks require a reduced number of pilot beams for sparse signal recovery using compressed measurements. However, both the ASE and BER degraded upon increasing the frequency as well as the transmission distance, which became particularly pronounced at certain specific frequencies, where the molecular absorption was extremely high.

APPENDIX A

PROOF OF LEMMA 1

The total coherence $\mu^t(\tilde{\Phi})$ of the equivalent sensing matrix $\tilde{\Phi}$ is defined as [38], [39]

$$\mu^t(\tilde{\Phi}) = \sum_{i=1}^{G_R G_T} \sum_{j=1, j \neq i}^{G_R G_T} \left| \tilde{\Phi}_i^H \tilde{\Phi}_j \right|^2,$$

where the quantities $\tilde{\Phi}_i$ and $\tilde{\Phi}_j$ represent the i th and j th columns, respectively, of the matrix $\tilde{\Phi}$. Note that it can be bounded as follows:

$$\mu^t(\tilde{\Phi}) \leq \left\| \tilde{\Phi} \tilde{\Phi}^H \right\|_F^2 = \sum_{i=1}^{G_R G_T} \sum_{j=1}^{G_R G_T} \left| \tilde{\Phi}_i^H \tilde{\Phi}_j \right|^2.$$

Substituting $\tilde{\mathbf{F}} = \mathbf{X}_p^T \mathbf{F}_{\text{RF}}^T \mathbf{A}_T^*(\Phi_T)$ and $\tilde{\mathbf{W}} = \mathbf{W}_{\text{BB}}^H \mathbf{W}_{\text{RF}}^H \mathbf{A}_R(\Phi_R)$ in (30), one can rewrite the above bound as

$$\mu^t(\tilde{\Phi}) \leq \left\| \left(\tilde{\mathbf{F}} \tilde{\mathbf{F}}^H \right) \otimes \left(\tilde{\mathbf{W}} \tilde{\mathbf{W}}^H \right) \right\|_F^2. \quad (50)$$

Furthermore, employing the relationship $\|\mathbf{A} \otimes \mathbf{B}\|_F^2 = \|\mathbf{A}\|_F^2 \|\mathbf{B}\|_F^2$, one can simplify the above expression as

$$\mu^t(\tilde{\Phi}) \leq \left\| \tilde{\mathbf{F}} \tilde{\mathbf{F}}^H \right\|_F^2 \left\| \tilde{\mathbf{W}} \tilde{\mathbf{W}}^H \right\|_F^2 = \frac{G_T}{N_T} \|\mathbf{X}_p^T \mathbf{X}_p^*\|_F^2 \times \frac{G_R}{N_R} \|\mathbf{W}_{\text{BB}}^H \mathbf{W}_{\text{BB}}\|_F^2. \quad (51)$$

The simplification in the above result exploits the semi-unitary property of the matrices $\mathbf{A}_T(\Phi_T)$ and $\mathbf{A}_R(\Phi_R)$, respectively, given in (26), and owing to the choice of the RF TPC \mathbf{F}_{RF} and RC \mathbf{W}_{RF} as the DFT matrices. From (51), it can be readily observed that minimization of the total coherence $\mu^t(\tilde{\Phi})$ can be achieved by the minimization of the quantities $\|\mathbf{X}_p^T \mathbf{X}_p^*\|_F^2$ and $\|\mathbf{W}_{\text{BB}}^H \mathbf{W}_{\text{BB}}\|_F^2$, with respect to the pilot matrix \mathbf{X}_p and the baseband RC matrix \mathbf{W}_{BB} , respectively. The optimal pilot matrix \mathbf{X}_p subject to a suitable training power constraint can now be derived as follows.

Note that minimization of $\|\mathbf{X}_p^T \mathbf{X}_p^*\|_F^2$ is equivalent to the minimization of $\|\mathbf{X}_{p,i}^T \mathbf{X}_{p,i}^*\|_F^2$ with respect to each $\mathbf{X}_{p,i}$, $1 \leq i \leq N_F$, since the pilot matrix \mathbf{X}_p is block diagonal. Therefore, the optimal pilot matrix design optimization problem can be formulated as

$$\min_{\mathbf{X}_{p,i}} \|\mathbf{X}_{p,i}^T \mathbf{X}_{p,i}^*\|_F^2, \quad \text{s.t. } \|\mathbf{X}_{p,i}\|_F^2 = \frac{M_T}{N_F}. \quad (52)$$

The closed-form solution of the above problem can be derived as follows. Let $\mathbf{X}_{p,i} = \mathbf{U} \Sigma \mathbf{V}_1^H$ represent the SVD of the pilot matrix $\mathbf{X}_{p,i}$, where the matrices \mathbf{U} and \mathbf{V}_1 are unitary matrices of size $N_{\text{RF}} \times N_{\text{RF}}$ and $\frac{M_T}{N_F} \times \frac{M_T}{N_F}$, respectively. Since $M_T \leq N_T$, which implies that $\frac{M_T}{N_F} = \frac{M_T N_{\text{RF}}}{N_T} \leq N_{\text{RF}}$, the singular matrix $\Sigma \in \mathbb{C}^{N_{\text{RF}} \times \frac{M_T}{N_F}}$ has the following structure

$$\Sigma = \left[\text{diag} \left(\sigma_1, \dots, \sigma_{\frac{M_T}{N_F}} \right) \quad \mathbf{0}_{\frac{M_T}{N_F} \times N_{\text{RF}} - \frac{M_T}{N_F}} \right]^T, \quad (53)$$

where $\sigma_1, \dots, \sigma_{\frac{M_T}{N_F}}$ denote the singular values of the pilot matrix $\mathbf{X}_{p,i}$. Exploiting now the property of the unitary matrices \mathbf{U} and \mathbf{V}_1 , and the expression of the singular matrix Σ defined in (53), the optimization problem in (52) can be reformulated as

$$\min_{\sigma_i, 1 \leq \sigma_i \leq \frac{M_T}{N_F}} \sum_{i=1}^{\frac{M_T}{N_F}} \sigma_i^4, \quad \text{s.t. } \sum_{i=1}^{\frac{M_T}{N_F}} \sigma_i^2 = \frac{M_T}{N_F}. \quad (54)$$

Using the KKT conditions [52] for solving the above optimization problem, the solution is obtained as $\sigma_i^{\text{opt}} = 1$, $1 \leq i \leq \frac{M_T}{N_F}$. Substituting the values of σ_i^{opt} into the singular matrix of (53), followed by employing the resultant expression in the SVD of the pilot matrix $\mathbf{X}_{p,i}$ yields

$$\mathbf{X}_{p,i} = \mathbf{U} \left[\mathbf{I}_{\frac{M_T}{N_F}} \quad \mathbf{0}_{\frac{M_T}{N_F} \times N_{\text{RF}} - \frac{M_T}{N_F}} \right]^T \mathbf{V}_1^H, \quad (55)$$

which is the desired result. The optimal RC matrix \mathbf{W}_{BB} can also be derived following similar lines. ■

APPENDIX B
PROOF OF LEMMA 2

The Expectation-step (E-step) used for determining the conditional expectation of the log-likelihood function $\mathcal{L}(\Gamma|\hat{\Gamma}^{(j-1)})$ is given as

$$\begin{aligned}\mathcal{L}(\Gamma|\hat{\Gamma}^{(j-1)}) &= \mathbb{E}_{\mathbf{h}_b|\mathbf{y};\hat{\Gamma}^{(j-1)}} \{\log f(\mathbf{y}, \mathbf{h}_b; \Gamma)\} \\ &= \mathbb{E}_{\mathbf{h}_b|\mathbf{y};\hat{\Gamma}^{(j-1)}} \{\log [f(\mathbf{y}|\mathbf{h}_b)]\} + \mathbb{E}_{\mathbf{h}_b|\mathbf{y};\hat{\Gamma}^{(j-1)}} \{\log [f(\mathbf{h}_b; \Gamma)]\}.\end{aligned}\quad (56)$$

The term inside the first $\mathbb{E}\{\cdot\}$ operator can be simplified as

$$\log f(\mathbf{y}|\mathbf{h}_b) = -M_T M_R \log(\pi) - \log[\det(\mathbf{R}_v)] - (\mathbf{y} - \tilde{\Phi}\mathbf{h}_b)^H \mathbf{R}_v^{-1} (\mathbf{y} - \tilde{\Phi}\mathbf{h}_b), \quad (57)$$

which is seen to be independent of the hyperparameter matrix Γ . Therefore, the subsequent Maximization-step (M-step) can ignore this term, while maximizing the likelihood $\mathcal{L}(\Gamma|\hat{\Gamma}^{(j-1)})$ in (56). The equivalent optimization problem in the M-step follows as

$$\hat{\Gamma}^{(j)} = \arg \max_{\Gamma} \mathbb{E}_{\mathbf{h}_b|\mathbf{y};\hat{\Gamma}^{(j-1)}} \{\log [f(\mathbf{h}_b; \Gamma)]\}. \quad (58)$$

Upon substituting $f(\mathbf{h}_b; \Gamma)$ from (32) into the above optimization objective, the maximization problem can be decoupled into separate maximization problems with respect to the individual hyperparameters γ_i as

$$\hat{\gamma}_i^{(j)} = \arg \max_{\gamma_i} \left[-\log(\gamma_i) - \frac{\mathbb{E}_{\mathbf{h}_b|\mathbf{y};\hat{\Gamma}^{(j-1)}} \{|\mathbf{h}_b(i)|^2\}}{\gamma_i} \right]. \quad (59)$$

Solving the above problem yields the estimates $\hat{\gamma}_i^{(j)}$ as

$$\hat{\gamma}_i^{(j)} = \mathbb{E}_{\mathbf{h}_b|\mathbf{y};\hat{\Gamma}^{(j-1)}} \{|\mathbf{h}_b(i)|^2\}. \quad (60)$$

To simplify the conditional expectation $\mathbb{E}_{\mathbf{h}_b|\mathbf{y};\hat{\Gamma}^{(j-1)}} \{\cdot\}$ above, the *a posteriori* Probability Density Function (PDF) $f(\mathbf{h}_b|\mathbf{y};\hat{\Gamma}^{(j-1)})$ of \mathbf{h}_b can be expressed as [48]: $f(\mathbf{h}_b|\mathbf{y};\hat{\Gamma}^{(j-1)}) = \mathcal{CN}(\boldsymbol{\mu}_b^{(j)}, \mathbf{R}_b^{(j)})$, where the quantities $\boldsymbol{\mu}_b^{(j)} \in \mathbb{C}^{G_R G_T \times 1}$ and $\mathbf{R}_b^{(j)} \in \mathbb{C}^{G_R G_T \times G_R G_T}$ are defined as

$$\boldsymbol{\mu}_b^{(j)} = \mathbf{R}_b^{(j)} \tilde{\Phi}^H \mathbf{R}_v^{-1} \mathbf{y}, \quad \mathbf{R}_b^{(j)} = \left[\tilde{\Phi}^H \mathbf{R}_v^{-1} \tilde{\Phi} + \left(\hat{\Gamma}^{(j-1)} \right)^{-1} \right]^{-1}, \quad (61)$$

which represent the *a posteriori* mean vector and covariance matrix, respectively, of the beamspace channel \mathbf{h}_b . Employing the *a posteriori* PDF $f(\mathbf{h}_b|\mathbf{y};\hat{\Gamma}^{(j-1)})$, the expression in (60) can be simplified to

$$\hat{\gamma}_i^{(j)} = \mathbf{R}_b^{(j)}(i, i) + \left| \boldsymbol{\mu}_b^{(j)}(i) \right|^2, \quad (62)$$

which is the desired expression. ■

APPENDIX C

DERIVATION OF THE HYBRID MMSE RC

In order to derive the required expression, one can simplify the objective function of the optimization problem given in (46) as

$$\begin{aligned} \mathbb{E} \left\{ \|\bar{\mathbf{x}} - \bar{\mathbf{W}}_{\text{BB}}^H \bar{\mathbf{W}}_{\text{RF}}^H \mathbf{y}\|_2^2 \right\} &= \mathbb{E} \left\{ \text{Tr} \left[(\bar{\mathbf{x}} - \bar{\mathbf{W}}_{\text{BB}}^H \bar{\mathbf{W}}_{\text{RF}}^H \mathbf{y}) (\bar{\mathbf{x}} - \bar{\mathbf{W}}_{\text{BB}}^H \bar{\mathbf{W}}_{\text{RF}}^H \mathbf{y})^H \right] \right\} \\ &= \text{Tr} \left[\mathbb{E} \{ \bar{\mathbf{x}} \bar{\mathbf{x}}^H \} \right] - 2 \text{Re} \left\{ \text{Tr} \left[\mathbb{E} \{ \bar{\mathbf{x}} \mathbf{y}^H \} \bar{\mathbf{W}}_{\text{RF}} \bar{\mathbf{W}}_{\text{BB}} \right] \right\} \\ &\quad + \text{Tr} \left[\bar{\mathbf{W}}_{\text{BB}}^H \bar{\mathbf{W}}_{\text{RF}}^H \mathbb{E} \{ \mathbf{y} \mathbf{y}^H \} \bar{\mathbf{W}}_{\text{RF}} \bar{\mathbf{W}}_{\text{BB}} \right]. \end{aligned} \quad (63)$$

Since, the minimization is performed with respect to $(\bar{\mathbf{W}}_{\text{RF}}, \bar{\mathbf{W}}_{\text{BB}})$, one can neglect the first term $\text{Tr} \left[\mathbb{E} \{ \bar{\mathbf{x}} \bar{\mathbf{x}}^H \} \right]$. In order to further simplify (63), one can add the constant term $\text{Tr} \left[\bar{\mathbf{W}}_{\text{M}}^H \mathbb{E} \{ \mathbf{y} \mathbf{y}^H \} \bar{\mathbf{W}}_{\text{M}} \right]$ in the above expression, where the optimal MMSE RC $\bar{\mathbf{W}}_{\text{M}}$ obeys $\bar{\mathbf{W}}_{\text{M}}^H = \mathbb{E} \{ \bar{\mathbf{x}} \mathbf{y}^H \} \mathbb{E} \{ \mathbf{y} \mathbf{y}^H \}^{-1}$.

Finally, the above expression can be reformulated as

$$\begin{aligned} \mathbb{E} \left\{ \|\bar{\mathbf{x}} - \bar{\mathbf{W}}_{\text{BB}}^H \bar{\mathbf{W}}_{\text{RF}}^H \mathbf{y}\|_2^2 \right\} &= \text{Tr} \left[\bar{\mathbf{W}}_{\text{M}}^H \mathbb{E} \{ \mathbf{y} \mathbf{y}^H \} \bar{\mathbf{W}}_{\text{M}} \right] - 2 \text{Re} \left\{ \text{Tr} \left[\bar{\mathbf{W}}_{\text{M}}^H \mathbb{E} \{ \mathbf{y} \mathbf{y}^H \} \bar{\mathbf{W}}_{\text{RF}} \bar{\mathbf{W}}_{\text{BB}} \right] \right\} \\ &\quad + \text{Tr} \left[\bar{\mathbf{W}}_{\text{BB}}^H \bar{\mathbf{W}}_{\text{RF}}^H \mathbb{E} \{ \mathbf{y} \mathbf{y}^H \} \bar{\mathbf{W}}_{\text{RF}} \bar{\mathbf{W}}_{\text{BB}} \right] \\ &= \text{Tr} \left[(\bar{\mathbf{W}}_{\text{M}}^H - \bar{\mathbf{W}}_{\text{BB}}^H \bar{\mathbf{W}}_{\text{RF}}^H) \mathbb{E} \{ \mathbf{y} \mathbf{y}^H \} (\bar{\mathbf{W}}_{\text{M}}^H - \bar{\mathbf{W}}_{\text{BB}}^H \bar{\mathbf{W}}_{\text{RF}}^H)^H \right] \\ &= \left\| \mathbb{E} \{ \mathbf{y} \mathbf{y}^H \}^{1/2} (\bar{\mathbf{W}}_{\text{M}} - \bar{\mathbf{W}}_{\text{RF}} \bar{\mathbf{W}}_{\text{BB}}) \right\|_F^2, \end{aligned} \quad (64)$$

which is the desired expression. ■

REFERENCES

- [1] C. Han and Y. Chen, "Propagation modeling for wireless communications in the Terahertz band," *IEEE Communications Magazine*, vol. 56, no. 6, pp. 96–101, 2018.
- [2] Z. Chen, X. Ma, B. Zhang, Y. Zhang, Z. Niu, N. Kuang, W. Chen, L. Li, and S. Li, "A survey on Terahertz communications," *China Communications*, vol. 16, no. 2, pp. 1–35, 2019.
- [3] A. Faisal, H. Sardeddeen, H. Dahrouj, T. Y. Al-Naffouri, and M.-S. Alouini, "Ultramassive MIMO systems at Terahertz bands: Prospects and challenges," *IEEE Vehicular Technology Magazine*, vol. 15, no. 4, pp. 33–42, 2020.
- [4] J. M. Jornet and I. F. Akyildiz, "Channel modeling and capacity analysis for electromagnetic wireless nanonetworks in the Terahertz band," *IEEE Transactions on Wireless Communications*, vol. 10, no. 10, pp. 3211–3221, 2011.
- [5] H. Sardeddeen, M.-S. Alouini, and T. Y. Al-Naffouri, "An overview of signal processing techniques for Terahertz communications," *arXiv preprint arXiv:2005.13176*, 2020.
- [6] H. He, R. Wang, S. Jin, C.-K. Wen, and G. Y. Li, "Beamspace channel estimation in Terahertz communications: A model-driven unsupervised learning approach," *arXiv preprint arXiv:2006.16628*, 2020.
- [7] A. F. Molisch, V. V. Ratnam, S. Han, Z. Li, S. L. H. Nguyen, L. Li, and K. Haneda, "Hybrid beamforming for massive MIMO: A survey," *IEEE Communications magazine*, vol. 55, no. 9, pp. 134–141, 2017.

- [8] X. Zhang, A. F. Molisch, and S.-Y. Kung, "Variable-phase-shift-based RF-baseband codesign for MIMO antenna selection," *IEEE Transactions on Signal Processing*, vol. 53, no. 11, pp. 4091–4103, 2005.
- [9] R. M. Goody and Y. L. Yung, *Atmospheric radiation: theoretical basis*. Oxford university press, 1995.
- [10] L. S. Rothman, I. E. Gordon, A. Barbe, D. C. Benner, P. F. Bernath, M. Birk, V. Boudon, L. R. Brown, A. Campargue, J.-P. Champion *et al.*, "The HITRAN 2008 molecular spectroscopic database," *Journal of Quantitative Spectroscopy and Radiative Transfer*, vol. 110, no. 9-10, pp. 533–572, 2009.
- [11] C. Lin and G. Y. Li, "Adaptive beamforming with resource allocation for distance-aware multi-user indoor Terahertz communications," *IEEE Transactions on Communications*, vol. 63, no. 8, pp. 2985–2995, 2015.
- [12] S. Srivastava, J. Nath, and A. K. Jagannatham, "Data aided quasistatic and doubly-selective CSI estimation using affine-precoded superimposed pilots in millimeter wave MIMO-OFDM systems," *IEEE Transactions on Vehicular Technology*, vol. 70, no. 7, pp. 6983–6998, 2021.
- [13] A. Alkhateeb, O. El Ayach, G. Leus, and R. W. Heath, "Channel estimation and hybrid precoding for millimeter wave cellular systems," *IEEE Journal of Selected Topics in Signal Processing*, vol. 8, no. 5, pp. 831–846, 2014.
- [14] S. Srivastava, C. S. K. Patro, A. K. Jagannatham, and L. Hanzo, "Sparse, group-sparse, and online Bayesian learning aided channel estimation for doubly-selective mmwave hybrid MIMO OFDM systems," *IEEE Transactions on Communications*, vol. 69, no. 9, pp. 5843–5858, 2021.
- [15] O. El Ayach, S. Rajagopal, S. Abu-Surra, Z. Pi, and R. W. Heath, "Spatially sparse precoding in millimeter wave MIMO systems," *IEEE Transactions on Wireless Communications*, vol. 13, no. 3, pp. 1499–1513, 2014.
- [16] S. Srivastava, P. Sharma, S. Dwivedi, A. K. Jagannatham, and L. Hanzo, "Fast block LMS based estimation of angularly sparse channels for single-carrier wideband millimeter wave hybrid MIMO systems," *IEEE Transactions on Vehicular Technology*, vol. 70, no. 1, pp. 666–681, 2021.
- [17] X. Gao, L. Dai, S. Zhou, A. M. Sayeed, and L. Hanzo, "Wideband beamspace channel estimation for millimeter-wave MIMO systems relying on lens antenna arrays," *IEEE Transactions on Signal Processing*, vol. 67, no. 18, pp. 4809–4824, 2019.
- [18] P. Singh, S. Srivastava, A. K. Jagannatham, and L. Hanzo, "Second-order statistics-based semi-blind techniques for channel estimation in millimeter-wave MIMO analog and hybrid beamforming," *IEEE Transactions on Communications*, vol. 68, no. 11, pp. 6886–6901, 2020.
- [19] S. Srivastava, C. S. K. Patro, A. K. Jagannatham, and G. Sharma, "Sparse Bayesian learning (SBL)-based frequency-selective channel estimation for millimeter wave hybrid MIMO systems," in *2019 National Conference on Communications (NCC)*, 2019, pp. 1–6.
- [20] R. Guo, Y. Cai, M. Zhao, Q. Shi, B. Champagne, and L. Hanzo, "Joint design of beam selection and precoding matrices for mmwave MU-MIMO systems relying on lens antenna arrays," *IEEE Journal of Selected Topics in Signal Processing*, vol. 12, no. 2, pp. 313–325, 2018.
- [21] Y. Cai, Y. Xu, Q. Shi, B. Champagne, and L. Hanzo, "Robust joint hybrid transceiver design for millimeter wave full-duplex MIMO relay systems," *IEEE Transactions on Wireless Communications*, vol. 18, no. 2, pp. 1199–1215, 2019.
- [22] Y. Cai, K. Xu, A. Liu, M. Zhao, B. Champagne, and L. Hanzo, "Two-timescale hybrid analog-digital beamforming for mmwave full-duplex MIMO multiple-relay aided systems," *IEEE Journal on Selected Areas in Communications*, vol. 38, no. 9, pp. 2086–2103, 2020.
- [23] Q. Hu, Y. Cai, K. Kang, G. Yu, J. Hoydis, and Y. C. Eldar, "Two-timescale end-to-end learning for channel acquisition and hybrid precoding," *IEEE Journal on Selected Areas in Communications*, vol. 40, no. 1, pp. 163–181, 2022.
- [24] L. Yan, C. Han, and J. Yuan, "A dynamic array of sub-array architecture for hybrid precoding in the millimeter wave and

- Terahertz bands,” in *2019 IEEE International Conference on Communications Workshops (ICC Workshops)*. IEEE, 2019, pp. 1–5.
- [25] V. Schram, A. Moldovan, and W. H. Gerstacker, “Compressive sensing for indoor THz channel estimation,” in *2018 52nd Asilomar Conference on Signals, Systems, and Computers*. IEEE, 2018, pp. 1539–1546.
- [26] V. Schram, A. Bereyhi, J.-N. Zaech, R. R. Müller, and W. H. Gerstacker, “Approximate message passing for indoor THz channel estimation,” *arXiv preprint arXiv:1907.05126*, 2019.
- [27] X. Ma, Z. Chen, W. Chen, Z. Li, Y. Chi, C. Han, and S. Li, “Joint channel estimation and data rate maximization for intelligent reflecting surface assisted Terahertz MIMO communication systems,” *IEEE Access*, vol. 8, pp. 99 565–99 581, 2020.
- [28] X. Gao, L. Dai, Y. Zhang, T. Xie, X. Dai, and Z. Wang, “Fast channel tracking for Terahertz beamspace massive MIMO systems,” *IEEE Transactions on Vehicular Technology*, vol. 66, no. 7, pp. 5689–5696, 2016.
- [29] Y. Zhou, P. C. Yip, and H. Leung, “Tracking the direction-of-arrival of multiple moving targets by passive arrays: Algorithm,” *IEEE Transactions on Signal Processing*, vol. 47, no. 10, pp. 2655–2666, 1999.
- [30] G. Stratidakis, A.-A. A. Boulogeorgos, and A. Alexiou, “A cooperative localization-aided tracking algorithm for THz wireless systems,” in *2019 IEEE Wireless Communications and Networking Conference (WCNC)*. IEEE, 2019, pp. 1–7.
- [31] G. Stratidakis, G. D. Ntouni, A.-A. A. Boulogeorgos, D. Kritharidis, and A. Alexiou, “A low-overhead hierarchical beam-tracking algorithm for THz wireless systems,” in *2020 European Conference on Networks and Communications (EuCNC)*. IEEE, 2020, pp. 74–78.
- [32] N. Kaur, S. S. Hosseini, and B. Champagne, “Enhanced channel tracking in THz beamspace massive MIMO: A deep CNN approach,” in *2020 Asia-Pacific Signal and Information Processing Association Annual Summit and Conference (APSIPA ASC)*. IEEE, 2020, pp. 76–81.
- [33] D. He, Z. Wang, T. Q. S. Quek, S. Chen, and L. Hanzo, “Deep learning-assisted Terahertz QPSK detection relying on single-bit quantization,” *IEEE Transactions on Communications*, 10.1109/TCOMM.2021.3112216.
- [34] K. Dovelos, M. Matthaïou, H. Q. Ngo, and B. Bellalta, “Channel estimation and hybrid combining for wideband Terahertz massive MIMO systems,” *IEEE Journal on Selected Areas in Communications*, vol. 39, no. 6, pp. 1604–1620, 2021.
- [35] Z. Sha and Z. Wang, “Channel estimation and equalization for Terahertz receiver with RF impairments,” *IEEE Journal on Selected Areas in Communications*, vol. 39, no. 6, pp. 1621–1635, 2021.
- [36] E. Balevi and J. G. Andrews, “Wideband channel estimation with a generative adversarial network,” *IEEE Transactions on Wireless Communications*, vol. 20, no. 5, pp. 3049–3060, 2021.
- [37] C. Lin and G. Y. Li, “Indoor Terahertz communications: How many antenna arrays are needed?” *IEEE Transactions on Wireless Communications*, vol. 14, no. 6, pp. 3097–3107, 2015.
- [38] M. Elad, “Optimized projections for compressed sensing,” *IEEE Transactions on Signal Processing*, vol. 55, no. 12, pp. 5695–5702, 2007.
- [39] G. Li, Z. Zhu, D. Yang, L. Chang, and H. Bai, “On projection matrix optimization for compressive sensing systems,” *IEEE Transactions on Signal Processing*, vol. 61, no. 11, pp. 2887–2898, 2013.
- [40] H. Yuan, N. Yang, K. Yang, C. Han, and J. An, “Hybrid beamforming for MIMO-OFDM Terahertz wireless systems over frequency selective channels,” in *2018 IEEE Global Communications Conference (GLOBECOM)*. IEEE, 2018, pp. 1–6.
- [41] S. Srivastava, A. Mishra, A. K. Jagannatham, and G. Ascheid, “SBL-based hybrid precoder/ combiner design for power and spectrally efficient millimeter wave MIMO systems,” in *2020 International Conference on Signal Processing and Communications (SPCOM)*, 2020, pp. 1–5.
- [42] M. Majumder, H. Saxena, S. Srivastava, and A. K. Jagannatham, “Optimal bit allocation-based hybrid precoder-combiner design techniques for mmwave MIMO-OFDM systems,” *IEEE Access*, vol. 9, pp. 54 109–54 125, 2021.

- [43] C. Hill. (1999) HITRAN online interface to the HITRAN database. [Online]. Available: <https://hitran.org>
- [44] R. Piesiewicz, C. Jansen, D. Mittleman, T. Kleine-Ostmann, M. Koch, and T. Kurner, "Scattering analysis for the modeling of THz communication systems," *IEEE Transactions on Antennas and Propagation*, vol. 55, no. 11, pp. 3002–3009, 2007.
- [45] J. H. Van Vleck and V. F. Weisskopf, "On the shape of collision-broadened lines," *Reviews of Modern Physics*, vol. 17, no. 2-3, p. 227, 1945.
- [46] H. Zhang and F. Ding, "On the Kronecker products and their applications," *Journal of Applied Mathematics*, vol. 2013, 2013.
- [47] D. P. Wipf and B. D. Rao, "Sparse Bayesian learning for basis selection," *IEEE Transactions on Signal processing*, vol. 52, no. 8, pp. 2153–2164, 2004.
- [48] S. M. Kay, *Fundamentals of statistical signal processing*. Prentice Hall PTR, 1993.
- [49] D. Tse and P. Viswanath, *Fundamentals of Wireless Communication*. Cambridge university press, 2005.
- [50] D. P. Wipf and B. D. Rao, "An empirical Bayesian strategy for solving the simultaneous sparse approximation problem," *IEEE Transactions on Signal Processing*, vol. 55, no. 7, pp. 3704–3716, 2007.
- [51] H. L. Van Trees and K. L. Bell, "Bayesian bounds for parameter estimation and nonlinear filtering/tracking," *AMC*, vol. 10, p. 12, 2007.
- [52] S. Boyd, S. P. Boyd, and L. Vandenberghe, *Convex optimization*. Cambridge university press, 2004.
- [53] S. Priebe, M. Jacob, and T. Kuerner, "AoA, AoD and ToA characteristics of scattered multipath clusters for THz indoor channel modeling," in *17th European Wireless 2011-Sustainable Wireless Technologies*. VDE, 2011, pp. 1–9.
- [54] I. F. Gorodnitsky and B. D. Rao, "Sparse signal reconstruction from limited data using FOCUSS: A re-weighted minimum norm algorithm," *IEEE Transactions on Signal Processing*, vol. 45, no. 3, pp. 600–616, 1997.
- [55] M. Al-Shoukairi, P. Schniter, and B. D. Rao, "A GAMP-based low complexity sparse Bayesian learning algorithm," *IEEE Transactions on Signal Processing*, vol. 66, no. 2, pp. 294–308, 2017.
- [56] C. Huang, L. Liu, C. Yuen, and S. Sun, "Iterative channel estimation using LSE and sparse message passing for mmwave MIMO systems," *IEEE Transactions on Signal Processing*, vol. 67, no. 1, pp. 245–259, 2019.
- [57] L. Wei, C. Huang, G. C. Alexandropoulos, C. Yuen, Z. Zhang, and M. Debbah, "Channel estimation for RIS-empowered multi-user MISO wireless communications," *IEEE Transactions on Communications*, vol. 69, no. 6, pp. 4144–4157, 2021.